PTEP

Prog. Theor. Exp. Phys. **2022** 023D03(32 pages)
DOI: 10.1093/ptep/ptac008

The mean-square radius of the neutron distribution in the relativistic and non-relativistic mean-field models

Haruki Kurasawa[1] and Toshio Suzuki[2,*]

[1]*Department of Physics, Graduate School of Science, Chiba University, Chiba 263-8522, Japan*
[2]*Research Center for Electron Photon Science, Tohoku University, Sendai 982-0826, Japan*
*E-mail: kt.suzuki2th@gmail.com

Received October 14, 2021; Revised December 27, 2021; Accepted January 11, 2022; Published January 14, 2022

It is investigated why the root-mean-square radius of the point neutron distribution is smaller by about 0.1 fm in non-relativistic mean-field models than in relativistic ones. The difference is shown to stem from the different values of the product of the effective mass and the strength of the one-body potential in the two frameworks. The values of those quantities are constrained by the Hugenholtz–Van Hove theorem. The neutron skin is not a simple function of the symmetry potential, but depends on the nucleon effective mass.

Subject Index D11, D12

1. Introduction

Recently much has been written on the neutron distribution in nuclei [1–5]. It is one of the most fundamental problems in nuclear physics together with the proton distribution [1,6]. The neutron distribution, however, has not been well determined experimentally so far. This is because the neutron density has been studied through hadron probes, where the ambiguity as to the interaction and the reaction mechanism is not avoidable yet [3].

In contrast to the neutron distribution, the proton distribution has been widely investigated throughout the periodic table of stable nuclei theoretically [6] and experimentally [7]. The relationship between the point proton and charge density distributions is defined unambiguously [6,8]. The latter is deduced from electron scattering cross sections rather model independently [7], compared with the strong interaction, since the electromagnetic interaction is well understood, and is so weak that the density distribution of the nuclear ground state is not disturbed [6,9].

It has been believed for a long time that electron scattering is useless in the study of neutron distribution in nuclei [6,10]. Recently, the present authors have proposed a new way to deduce the neutron distribution from electron scattering data [8]. They have derived an exact expression for the nth-order moment of the nuclear charge distribution and shown that the mean-square radius (msr) of the charge distribution (R_c^2) is dominated by the msr of the point proton distribution (R_p^2) and is independent of the neutron's msr (R_n^2), but that the nth-order ($n \geq 4$) moment of the charge density depends on the $(n-2)$th-order moment of the neutron distribution [8]. For example, the fourth-order moment of the charge density (Q_c^4) depends on R_n^2. Their relationship is uniquely defined, and the value of Q_c^4 is well determined in electron scattering experiments [7,11]. The value of R_n^2, however, is not separated from Q_c^4 experimentally. In order to deduce the value of R_n^2 from the experimental value of Q_c^4, it is necessary to

© The Author(s) 2022. Published by Oxford University Press on behalf of the Physical Society of Japan.
This is an Open Access article distributed under the terms of the Creative Commons Attribution License (https://creativecommons.org/licenses/by/4.0/), which permits unrestricted reuse, distribution, and reproduction in any medium, provided the original work is properly cited.

Downloaded from https://academic.oup.com/ptep/article/2022/2/023D03/6507566 by Deutsches Elektronen Synchrotron DESY user on 23 March 2022

rely on a model-dependent analysis. One advantage of using Q_c^4 for deducing the value of R_n^2 is that we need not be concerned with assumptions about the interaction and reaction mechanism in electron scattering, but are able to focus on the model dependence on nuclear structure.

At present, the nuclear structure is not investigated without invoking phenomenological models. Moreover, most of the models are constructed for different purposes independently. Hence, it is not appropriate for the separation of R_n^2 from Q_c^4 to choose one model among the many existing models. The present authors [4] have proposed the least-squares analysis (LSA) for the separation by employing as many previous models as possible together. Through the LSA, they explore the constraints that are inherent in the framework of the nuclear models. The procedure of the separation is as follows. First R_n^2 and Q_c^4 are calculated using several models in the same framework, and then the least-square line (LSL) for those values is obtained in the R_n^2–Q_c^4 plane. Next, the value of R_n^2 in the framework is determined by the cross point of the LSL and the line of Q_c^4 corresponding to its experimental value. In order to confirm the obtained result, the LSA of R_n^2 against the other moments has also been performed. The estimated values of R_n^2 are not model independent, but are derived on the basis of the data from the well known electromagnetic probe, utilizing the knowledge on the phenomenological models accumulated over a long time in nuclear physics. A similar method has been proposed for analyzing parity-violating electron scattering [2], and actually employed in the analysis of the recent JLab experiment [5,12].

In Ref. [4], the values of R_n^2 in ^{40}Ca, ^{48}Ca, and ^{208}Pb have been estimated, for which experimental values of Q_c^4 are available at present. They have arbitrarily chosen 11 relativistic and 9 non-relativistic models among more than 100 versions accumulated over the last 50 years [13–16]. These models well reproduce fundamental nuclear properties within the mean-field framework, assuming some nuclei to be doubly closed shell nuclei. The LSL is obtained with a small standard deviation and the values of R_n^2 are determined within the 1% error including the experimental one [4]. In this analysis, it has been shown that the relativistic and non-relativistic frameworks yield different values of R_n^2 from each other in ^{48}Ca and ^{208}Pb. The value of R_n in the non-relativistic models is smaller by about 0.1 fm than that in the relativistic models in both nuclei. Since, in those mean-field models, the values of R_p are fixed so as to reproduce the experimental values, the neutron skin defined by $\delta R = R_n - R_p$ differs by about 0.1 fm in the two frameworks. The difference is not between the models but between the two frameworks, so that the result is apparently understood to reflect an essential difference between the structures of the two mean-field approximations.

It should be noted that 0.1 fm is not small for the neutron skin itself. As seen later, e.g., in ^{208}Pb, δR is 0.275 and 0.162 fm in the relativistic and non-relativistic models, respectively. Understanding the 0.1 fm difference may be important for the study of nuclear fission and fusion phenomena, which are sensitive to the structure of the nuclear surface [1,17]. Recent detailed calculations [18] may not neglect an order of 0.1 fm difference in describing asymmetric nuclei. The 0.1 fm difference has also been pointed out to be crucial in neutron star physics [3,18].

The purpose of the present paper is to investigate why the value of R_n^2 in the non-relativistic mean-field models is smaller than in the relativistic ones. The difference will be shown to stem mainly from the difference between the products of the effective mass and the strength of the one-body potential in the two frameworks. These two quantities are constrained in each frame-

Downloaded from https://academic.oup.com/ptep/article/2022/2/023D03/6507566 by Deutsches Elektronen Synchrotron DESY user on 23 March 2022

work by the Hugenholtz–Van Hove (HVH) theorem [19–21]. This theorem has been proved in the mean-field approximation in the non-relativistic framework for symmetric nuclear matter. As will be shown in the present paper, the theorem also holds in asymmetric nuclear matter in both relativistic and non-relativistic models, and is also numerically maintained in the mean-field approximation for finite nuclei.

In Section 2, the root msr R in the one-body potential will be discussed in order to derive an analytical expression of R in terms of the strength of the potential and the nucleon effective mass, using the Woods–Saxon and harmonic potentials. In Section 3, the equations of motion in the relativistic models will be shown to have the same structure as the Schrödinger equation in the non-relativistic models. In Section 4, the HVH theorem will be extended to asymmetric nuclear matter. In Section 5, the complexity of the mean-field models due to a large variety of interaction parameters will be simplified by using the Woods–Saxon-type function, aiming to make clear the difference between the relativistic and non-relativistic models. In Section 6, the difference between δR in the two frameworks will be investigated in detail, according to the HVH theorem. The final section will be devoted to a brief summary of the present paper.

2. The nuclear radius in the one-body potential

Many phenomenological models have been proposed with various interaction parameters [13,16]. Whether the nuclear radius (R) is R_n or R_p, it may be a complicated function of their parameters, and the function would be different from one model to another. The radius, however, is one of the most fundamental quantities that determine the structure of the nucleus, and, hence, R_c is used as an input to fix the free parameters of the models. This fact implies that the relationship of R with other key quantities of nuclei like those in the one-body potential must be almost the same in the mean-field models, although those key quantities may also depend on the parameters in complicated ways.

Such relationships of R with other key quantities should hold even in simplified one-body potential models, if they describe well the gross properties of nuclei [1]. As a simple example, the Woods–Saxon (WS) potential is most widely used in the literature [1]. It may also become a guide for the present purpose, if we have an analytical formula for the relationship between R and the parameters of the one-body Hamiltonian with the WS potential:

$$H = \frac{\boldsymbol{p}^2}{2M} + V_{\rm ws}(r), \quad V_{\rm ws}(r) = \frac{V_{\rm ws}}{1 + e^{(r-R_{\rm ws})/a_{\rm ws}}}. \tag{1}$$

Aiming to have an analytical expression of the relationship, we require the help of the harmonic oscillator (HO) potential,

$$V_{\rm H}(r) = \frac{k}{2}\left(r^2 - R_{\rm H}^2\right), \qquad k = M\omega^2, \tag{2}$$

$R_{\rm H}$ being a constant that determines the value of $V_{\rm H}(0)$. Bohr and Mottelson have shown that the single-particle wave functions in the WS potential, which determine the value of R, are well reproduced by those of the HO potential [1]. In the HO potential, the dimension analysis yields the expression of the radius $R_{\rm ho}$ as

$$R_{\rm ho} = \frac{C}{(Mk)^{1/4}} \tag{3}$$

with C denoting a constant. For the above exact formula, let us search for the expression of $R_{\rm ho}$ in terms of the WS parameters by minimizing the following quantity with respect to the

Downloaded from https://academic.oup.com/ptep/article/2022/2/023D03/6507566 by Deutsches Elektronen Synchrotron DESY user on 23 March 2022

variables, k and $R_{\rm H}$:

$$F_n(k, R_{\rm H}) = \int_0^{R_{\rm H}} dr\, r^n (V_{\rm H}(r) - V_{\rm ws}(r))^2, \tag{4}$$

where n is considered to be 0 for the surface integral and 2 for the volume integral. The value of n is chosen by referring to Ref. [1], which shows a similarity of the wave functions in the two potentials with $\omega = 8.6$ MeV and $V_{\rm H}(0) = -55$ MeV and with $V_{\rm ws} = -50$ MeV, $R_{\rm ws} = 5.8$ fm, and $a_{\rm ws} = 0.65$ fm. The numerical method yields the minimum values of F_n for the same WS parameters at $\omega = 8.63$ MeV and $V_{\rm H}(0) = -55.20$ MeV for $n = 0$, and at $\omega = 9.66$ MeV and $V_{\rm H}(0) = -62.65$ MeV for $n = 2$. Comparing these values with those in Ref. [1], it may be reasonable to employ $n = 0$, rather than $n = 2$, for reproducing the wave functions in the WS potential.

Once we determine the value of n, it is possible to derive an analytical formula for the approximate relationship between $R_{\rm ho}$ and the WS parameters. Equation (4) for $n = 0$ is written as

$$F_0(k, R_{\rm H}) = \int_0^{R_{\rm H}} dr (V_{\rm H}(r) - V_{\rm ws}(r))^2 = \frac{2}{15} k^2 R_{\rm H}^5 + F_{\rm H} + F_{\rm V},$$

where we have defined

$$F_{\rm H} = -2 \int_0^{R_{\rm H}} dr\, V_{\rm H}(r) V_{\rm ws}(r) = -k V_{\rm ws} \int_0^{\infty} dr\, \frac{r^2 - R_{\rm H}^2}{1 + e^{(r - R_{\rm ws})/a_{\rm ws}}} + \delta F_{\rm H}, \tag{5}$$

$$F_{\rm V} = \int_0^{R_{\rm H}} dr\, V_{\rm ws}^2(r) = V_{\rm ws}^2 \int_0^{\infty} \frac{dr}{(1 + e^{(r - R_{\rm ws})/a_{\rm ws}})^2} + \delta F_{\rm V}, \tag{6}$$

with

$$\delta F_{\rm H} = k V_{\rm ws} \int_{R_{\rm H}}^{\infty} dr\, \frac{r^2 - R_{\rm H}^2}{1 + e^{(r - R_{\rm ws})/a_{\rm ws}}}, \qquad \delta F_{\rm V} = -V_{\rm ws}^2 \int_{R_{\rm H}}^{\infty} \frac{dr}{(1 + e^{(r - R_{\rm ws})/a_{\rm ws}})^2}. \tag{7}$$

Using the identity for a general function $g(r)$,

$$\int_{R_{\rm H}}^{\infty} dr\, \frac{g(r)}{(1 + e^{(r - R_{\rm ws})/a_{\rm ws}})^n} = \Delta^n a_{\rm ws} \int_0^{\infty} dx\, \frac{g(a_{\rm ws} x + R_{\rm H}) e^{-nx}}{(1 + \Delta e^{-x})^n}, \quad \Delta = e^{-(R_{\rm H} - R_{\rm ws})/a_{\rm ws}},$$

we can neglect $\delta F_{\rm H}$ and $\delta F_{\rm V}$ in Eqs. (5) and (6), assuming $\Delta \ll 1$. Then, $F_{\rm V}$ in Eq. (6) is independent of k and $R_{\rm H}$, and it is enough to minimize only the first term on the rightmost side of Eq. (5). The integral of the first term is performed with the use of Sommerfeld expansion. In neglecting contributions of relative order $e^{-R_{\rm ws}/a_{\rm ws}}$ [1], it is written as

$$\int_0^{\infty} dr\, \frac{g(r)}{1 + e^{(r - R_{\rm ws})/a_{\rm ws}}} = \int_0^{R_{\rm ws}} dr\, g(r) + \frac{\pi^2 a_{\rm ws}^2}{6} g'(R_{\rm ws}) + \frac{7\pi^4 a_{\rm ws}^4}{360} g'''(R_{\rm ws}) + \cdots.$$

Since $g'''(r) = 0$ for Eq. (5), we have

$$F_0(k, R_{\rm H}) = \frac{2}{15} k^2 R_{\rm H}^5 + k V_{\rm ws} \left(R_{\rm H}^2 R_{\rm ws} - \frac{1 + b_{\rm ws}}{3} R_{\rm ws}^3 \right), \quad b_{\rm ws} = \left(\frac{\pi a_{\rm ws}}{R_{\rm ws}} \right)^2.$$

It should be noticed that there is no higher-order contribution from the diffuseness parameter. The partial differentials of the above equation F_0 with respect to k and $R_{\rm H}$ yield its minimum value at

$$k = -3 \left(\frac{3}{5} \right)^{3/2} \frac{V_{\rm ws}}{R_{\rm ws}^2 (1 + b_{\rm ws})^{3/2}},$$

$$R_{\rm H}^2 = \frac{5}{3}(1 + b_{\rm ws}) R_{\rm ws}^2, \qquad V_{\rm H}(0) = \frac{3}{2}\sqrt{\frac{3}{5}} \frac{V_{\rm ws}}{\sqrt{1 + b_{\rm ws}}}. \tag{8}$$

Downloaded from https://academic.oup.com/ptep/article/2022/2/023D03/6507566 by Deutsches Elektronen Synchrotron DESY user on 23 March 2022

When employing the values $V_{\rm ws} = -50$ MeV, $R_{\rm ws} = 5.8$ fm, and $a_{\rm ws} = 0.65$ fm in Ref. [1], the above equations provide $\omega = 8.49$ MeV and $V_{\rm H}(0) = -54.80$ MeV, which reproduce almost the same values obtained by the numerical method mentioned above.

Finally, inserting Eq. (8) into Eq. (3), $R_{\rm ho}$ is described approximately in terms of the WS parameters as

$$R_{\rm ho} \approx B\left(-\frac{R_{\rm ws}^2}{m^* V_{\rm ws}}\right)^{1/4}(1+b_{\rm ws})^{3/8}, \tag{9}$$

B being a constant. In the above equation, the nucleon mass has been replaced by the effective mass, $M^* = Mm^*$. Equation (9) expresses well our expectation such that the value of R increases with $R_{\rm ws}$, and decreases with increasing $(-V_{\rm ws})$ and m^*. Indeed, the first parenthesis on the right-hand side may be derived in the square-well potential with the depth $V_{\rm ws}$ and the width $R_{\rm ws}$. Equation (9) shows that the diffuseness parameter contributes to the radius in the form of $(a_{\rm ws}/R_{\rm ws})^2$.

If the neutron potential, V_n, and effective mass, m_n^*, are different from V_p and m_p^* of the proton, the value of R_n may be different from that of R_p. In the same way, if V_n and m_n^* in one model are different from those in another model, their R_n are different from each other. When comparing the nuclear radius R_1 in one framework with R_2 in another one, the following expression is useful:

$$\frac{R_1}{R_2} = \left(\frac{m_2^* V_{\rm ws,2}}{m_1^* V_{\rm ws,1}}\right)^{1/4}\left(\frac{R_{\rm ws,1}}{R_{\rm ws,2}}\right)^{1/2}\left(\frac{1+b_{\rm ws,1}}{1+b_{\rm ws,2}}\right)^{3/8}. \tag{10}$$

3. Equations of motion of the mean-field models

Equations (9) and (10) are simple enough to understand the relationship between $R_{\rm ho}$ and the key quantities of the one-body potential. The effective mass and the one-body potential are well defined quantities in the mean-field models. Expecting that such a simple relationship also holds approximately in those phenomenological models, let us investigate how they appear in the equations of motion in the relativistic and non-relativistic models.

In the relativistic nonlinear σ–ω–ρ model, the nuclear Lagrangian is given, using the notations in the literature [14,16,22], by

$$\begin{aligned}\mathcal{L} = {} & \overline{\psi}\left(i\gamma_\mu\partial^\mu - M - g_\sigma\sigma - g_\omega\gamma_\mu\omega^\mu - g_\rho\gamma_\mu\boldsymbol{\tau}\cdot\boldsymbol{b}^\mu - e\gamma_\mu A^\mu\frac{1+\tau_3}{2}\right)\psi \\ & + \frac{1}{2}(\partial_\mu\sigma)^2 - \frac{m_\sigma^2}{2}\sigma^2 - \frac{g_3}{3}\sigma^3 - \frac{g_4}{4}\sigma^4 - \frac{1}{4}\omega_{\mu\nu}\omega^{\mu\nu} + \frac{m_\omega^2}{2}\omega_\mu\omega^\mu + \frac{c_4}{4}(\omega_\mu\omega^\mu)^2 \\ & - \frac{1}{4}\boldsymbol{b}_{\mu\nu}\cdot\boldsymbol{b}^{\mu\nu} + \frac{m_\rho^2}{2}\boldsymbol{b}_\mu\cdot\boldsymbol{b}^\mu + \lambda g_\rho^2\boldsymbol{b}_\mu\cdot\boldsymbol{b}^\mu g_\omega^2\omega_\nu\omega^\nu - \frac{1}{4}A_{\mu\nu}A^{\mu\nu}.\end{aligned} \tag{11}$$

Then, the Euler–Lagrange equation provides us with the equations of motion for the static mean field:

$$(-i\boldsymbol{\alpha}\cdot\boldsymbol{\nabla} + \gamma_0(M+V_\sigma) + V_0)\psi = (E+M)\psi, \tag{12}$$

$$\left(-\boldsymbol{\nabla}^2 + m_\sigma^2\right)V_\sigma = -g_\sigma^2\left(\rho_S + \frac{g_3}{g_\sigma^3}V_\sigma^2 + \frac{g_4}{g_\sigma^4}V_\sigma^3\right), \tag{13}$$

$$\left(-\boldsymbol{\nabla}^2 + m_\omega^2\right)V_\omega = g_\omega^2\left(\rho - \frac{c_4}{g_\omega^4}V_\omega^3 - 2\lambda V_\omega V_\rho^2\right), \tag{14}$$

Downloaded from https://academic.oup.com/ptep/article/2022/2/023D03/6507566 by Deutsches Elektronen Synchrotron DESY user on 23 March 2022

Table 1. The root msr of the point neutron (R_n) and proton (R_p) distributions calculated with NL3 for ^{48}Ca and ^{208}Pb. The numbers are given in units of fm, except for those in parentheses, which denote the ratio to R_τ. For details, see the text.

	R_n	$(R_n)_G$	$(R_n)_N$	R_p	$(R_p)_G$	$(R_p)_N$
^{48}Ca	3.6050	3.5736(0.991)	3.6082(1.001)	3.3789	3.3522(0.992)	3.3846(1.002)
^{208}Pb	5.7405	5.6888(0.991)	5.7522(1.002)	5.4600	5.4135(0.991)	5.4656(1.001)

$$\left(-\nabla^2 + m_\rho^2\right) V_\rho = g_\rho^2 \left(\rho_p - \rho_n - 2\lambda V_\omega^2 V_\rho\right), \tag{15}$$

$$-\nabla^2 V_c = e^2 \rho_p. \tag{16}$$

In Eqs. (12)–(16), we have defined ψ as a single-particle wave function and used the following notations: $V_\sigma = g_\sigma \sigma$, $V_\omega = g_\omega \omega^0$, $V_\rho = g_\rho b_3^0$, and V_c for the Coulomb potential, $V_c = eA^0$. Moreover, V_0 is given by

$$V_0(\boldsymbol{r}) = V_\omega(\boldsymbol{r}) + V_\rho(\boldsymbol{r})\tau_3 + V_c(\boldsymbol{r})\frac{1+\tau_3}{2} \tag{17}$$

with $\tau_3 = +1(-1)$ for protons (neutrons), and the nucleon densities are

$$\rho_S(\boldsymbol{r}) = \sum_\alpha \overline{\psi}_\alpha(\boldsymbol{r})\psi_\alpha(\boldsymbol{r}), \quad \rho_\tau(\boldsymbol{r}) = \sum_{\alpha\in\tau} \psi_\alpha^\dagger(\boldsymbol{r})\psi_\alpha(\boldsymbol{r}), \quad \rho(\boldsymbol{r}) = \rho_n(\boldsymbol{r}) + \rho_p(\boldsymbol{r}),$$

with $\tau = p$ for protons and $\tau = n$ for neutrons.

Equation (12) represents two coupled equations for the upper component, $\psi_u(\boldsymbol{r})$, and the lower two components, $\psi_d(\boldsymbol{r})$, of $\psi(\boldsymbol{r})$. One of them gives

$$\psi_d(\boldsymbol{r}) = -\frac{1}{2M_\tau^*(\boldsymbol{r})} i\boldsymbol{\sigma}\cdot\nabla\psi_u(\boldsymbol{r}), \tag{18}$$

writing the effective nucleon mass, $M_\tau^*(\boldsymbol{r})$, as

$$M_\tau^*(\boldsymbol{r}) = \frac{2M + E + V_\sigma(\boldsymbol{r}) - V_0(\boldsymbol{r})}{2}. \tag{19}$$

By inserting Eq. (18) into the other equation of Eq. (12), we obtain the Schrödinger-like equation as

$$\left(-\nabla\frac{1}{2M_\tau^*(\boldsymbol{r})}\cdot\nabla + V_\tau(\boldsymbol{r}) + V_c(\boldsymbol{r})\frac{1+\tau_3}{2} - i\left(\nabla\frac{1}{2M_\tau^*(\boldsymbol{r})}\right)\cdot(\nabla\times\boldsymbol{\sigma})\right)\psi_u(\boldsymbol{r}) = E\psi_u(\boldsymbol{r}). \tag{20}$$

In the above equation, the nuclear potential, $V_\tau(\boldsymbol{r})$, is defined by

$$V_\tau(\boldsymbol{r}) = V_\sigma(\boldsymbol{r}) + V_\omega(\boldsymbol{r}) + V_\rho(\boldsymbol{r})\tau_3. \tag{21}$$

We note that the effective mass, $M_\tau^*(\boldsymbol{r})$, is written approximately as

$$M_\tau^*(\boldsymbol{r}) \approx M + \frac{1}{2}\left(V_\sigma(\boldsymbol{r}) - V_\omega(\boldsymbol{r}) - V_\rho(\boldsymbol{r})\tau_3 - V_c(\boldsymbol{r})\frac{1+\tau_3}{2}\right), \tag{22}$$

using the fact that $2M + E \approx 2M$. For ^{208}Pb, the values of the potentials around the center of the nuclear density are about $V_\sigma \approx -380$ MeV, $V_\omega \approx 306$ MeV, and $V_\rho \approx -6$ MeV [22]. It should be noted that the effective mass in the relativistic models is almost isoscalar, and is dominated by V_σ and V_ω in the same way as the spin–orbit potential in the last term on the left-hand side in Eq. (20).

The root msrs of the point proton and neutron distributions calculated with NL3 [22] are listed in Table 1. They are defined as

Downloaded from https://academic.oup.com/ptep/article/2022/2/023D03/6507566 by Deutsches Elektronen Synchrotron DESY user on 23 March 2022

$$R_\tau^2 = \frac{1}{N_\tau}\sum_{\alpha\in\tau}\int_0^\infty dr\, r^2\big(G_\alpha^2(r)+F_\alpha^2(r)\big)\,, \qquad (R_\tau)_G^2 = \frac{1}{N_\tau}\sum_{\alpha\in\tau}\int_0^\infty dr\, r^2 G_\alpha^2(r),$$

$$(R_\tau)_N^2 = \frac{1}{N_\tau}\sum_{\alpha\in\tau}\int_0^\infty dr\, r^2\frac{G_\alpha^2(r)}{n_G}\,, \qquad n_G = \int_0^\infty dr\, G_\alpha^2(r)\,,$$

where $G_\alpha(r)/r$ and $F_\alpha(r)/r$ denote the radial part of the large and small components of $\psi_\alpha(\boldsymbol{r})$, respectively, with the normalization $\int_0^\infty dr(G_\alpha^2(r)+F_\alpha^2(r))=1$. Moreover, we have defined $N_\tau = N(Z)$ for $\tau = n(p)$, and n_G for the normalization of the upper component used in $(R_\tau)_N^2$. Table 1 also shows the ratios of $(R_\tau)_G$ and $(R_\tau)_N$ to R_τ in the parentheses. As seen from $(R_\tau)_G$ in Table 1, the contribution of the lower component to R_τ is about 1%, and it is absorbed into $(R_\tau)_N$, which is calculated with the renormalized large component $G_\alpha(r)/\sqrt{n_G}$. Similar results are obtained in other relativistic models. According to these results, we will use the renormalized large component, ignoring the small component, when comparing the relativistic models with the non-relativistic ones below.

We note that, in principle, the two-component framework equivalent to the four-component one should be derived by the Foldy–Wouthuysen unitary transformation [9]. In order to obtain the normalized two-component wave functions, Eq. (20) will only be used in the present paper for comparison with non-relativistic models, for simplicity and transparency. In Ref. [4], calculations of the msr in the relativistic models were performed within the four-component framework.

In the Skyrme–Hartree–Fock approximation in the non-relativistic models, the Schrödinger equation is written as [23,24]

$$\left(-\boldsymbol{\nabla}\frac{1}{2M_\tau^*(\boldsymbol{r})}\cdot\boldsymbol{\nabla} + V_\tau(\boldsymbol{r}) + V_c(\boldsymbol{r})\frac{1+\tau_3}{2} - i\boldsymbol{W}_\tau(\boldsymbol{r})\cdot(\boldsymbol{\nabla}\times\boldsymbol{\sigma})\right)\varphi(\boldsymbol{r}) = E\varphi(\boldsymbol{r}), \tag{23}$$

where, using the same notations as in Ref. [24], $M_\tau^*(\boldsymbol{r})$, $V_\tau(\boldsymbol{r})$, and $\boldsymbol{W}_\tau(\boldsymbol{r})$ are given as

$$\frac{1}{M_\tau^*(\boldsymbol{r})} = \frac{1}{M} + \frac{t_1(2+x_1)+t_2(2+x_2)}{4}\rho(\boldsymbol{r}) + \frac{t_2(1+2x_2)-t_1(1+2x_1)}{4}\rho_\tau(\boldsymbol{r})\,, \tag{24}$$

$$\begin{aligned} V_\tau(\boldsymbol{r}) = {}& \frac{t_0}{2}((2+x_0)\rho(\boldsymbol{r}) - (1+2x_0)\rho_\tau(\boldsymbol{r})) + \frac{t_3}{24}(2+x_3)(2+\alpha)\rho^{\alpha+1}(\boldsymbol{r}) \\ & - \frac{t_3}{24}(2x_3+1)\big[2\rho^\alpha(\boldsymbol{r})\rho_\tau(\boldsymbol{r}) + \alpha\rho^{\alpha-1}(\boldsymbol{r})\big(\rho_p^2(\boldsymbol{r})+\rho_n^2(\boldsymbol{r})\big)\big] \\ & + \frac{t_1(2+x_1)+t_2(2+x_2)}{8}K(\boldsymbol{r}) + \frac{t_2(1+2x_2)-t_1(1+2x_1)}{8}K_\tau(\boldsymbol{r}) \\ & + \frac{t_2(2+x_2)-3t_1(2+x_1)}{16}\nabla^2\rho(\boldsymbol{r}) + \frac{3t_1(1+2x_1)+t_2(1+2x_2)}{16}\nabla^2\rho_\tau(\boldsymbol{r}) \\ & - \frac{W_0}{2}\boldsymbol{\nabla}\cdot(\boldsymbol{J}(\boldsymbol{r})+\boldsymbol{J}_\tau(\boldsymbol{r})), \end{aligned} \tag{25}$$

$$\begin{aligned} \boldsymbol{W}_\tau(\boldsymbol{r}) &= \frac{W_0}{2}\boldsymbol{\nabla}(\rho(\boldsymbol{r})+\rho_\tau(\boldsymbol{r})) + \frac{t_1-t_2}{8}\boldsymbol{J}_\tau(\boldsymbol{r}) - \frac{t_1x_1+t_2x_2}{8}\boldsymbol{J}(\boldsymbol{r}) \\ &\approx \frac{W_0}{2}\boldsymbol{\nabla}(\rho(\boldsymbol{r})+\rho_\tau(\boldsymbol{r})). \end{aligned} \tag{26}$$

In Eq. (25), $K(\boldsymbol{r}) = K_n(\boldsymbol{r}) + K_p(\boldsymbol{r})$ has been defined with $K_\tau(\boldsymbol{r}) = \sum_{\alpha\in\tau}|\nabla\varphi_\alpha(\boldsymbol{r})|^2$, and $\boldsymbol{J}(\boldsymbol{r}) = \boldsymbol{J}_n(\boldsymbol{r}) + \boldsymbol{J}_p(\boldsymbol{r})$, where $\boldsymbol{J}_\tau(\boldsymbol{r})$ denotes the spin density given in Ref. [24].

It is seen that Eq. (23) in the non-relativistic models has the same structure as Eq. (20) in the relativistic models. They are composed of four parts, $M_\tau^*(\boldsymbol{r})$, $V_\tau(\boldsymbol{r})$, $V_c(\boldsymbol{r})$, and the spin–

Downloaded from https://academic.oup.com/ptep/article/2022/2/023D03/6507566 by Deutsches Elektronen Synchrotron DESY user on 23 March 2022

orbit potential. If the strengths and the coordinate dependences of these parts were the same in the two frameworks, one could not distinguish one framework from another, in spite of their complicated parameter sets. Among the four parts, the last two are expected to play a minor role in the present purpose to explore the difference between δR in the two frameworks. The Coulomb potential is almost the same, and the strengths of the spin–orbit potentials reproduce experimental values of the single-particle energy levels in both frameworks [14,25]. In contrast to these, the first two parts are strongly model dependent. The values of the effective masses are spread out over a wide range [13]. Similarly, there is no reason why the one-body potentials are almost the same in all the mean-field models. Hence, the 0.1 fm difference between δR may be related to $M^*_\tau(\boldsymbol{r})$ and $V_\tau(\boldsymbol{r})$ depending on the different interaction parameters.

This observation is consistent with Eqs. (9) and (10), which clearly indicate that the difference problem is related to the effective mass and one-body potential. It is also apparent that they are not independent of each other. On the one hand, the product of $M^*_p(\boldsymbol{r})$ and $V_p(\boldsymbol{r})$ is constrained by hand so as to reproduce the experimental value of R_c in both relativistic and non-relativistic models. On the other hand, there is not a similar constraint on the neutron distribution, but both frameworks predict values of R_n that are distributed within a narrow range around each average value [4]. If the difference between δR is actually related to the effective mass and the one-body potential, there should be another constraint on the variations of these two quantities that works differently in the relativistic and non-relativistic models.

It may be natural to expect the symmetry energy [2] to be one such candidate. The symmetry energy coefficient, a_4 [26], is composed of potential and kinetic parts [1], which are given in the present relativistic and non-relativistic mean-field models, respectively, as [13]

$$a_{4,\mathrm{rel}} = \frac{k_\mathrm{F}^2}{6\sqrt{k_\mathrm{F}^2 + M_\sigma^2}} + \frac{\rho}{2}\frac{g_\rho^2}{m_\rho^2 + 2\lambda g_\rho^2 V_\omega^2}, \qquad M_\sigma = M + V_\sigma, \tag{27}$$

$$a_{4,\mathrm{non}} = \left(\frac{3\pi^2}{2}\right)^{2/3}\left(\frac{\rho^{2/3}}{6M} + \frac{-3t_1x_1 + t_2(5x_2+4)}{24}\rho^{5/3}\right) - \frac{2x_0+1}{8}t_0\rho - \frac{2x_3+1}{48}t_3\rho^{\alpha+1}, \tag{28}$$

where k_F denotes the Fermi momentum and ρ the nucleon density in the nuclear matter. Actually, they are related to the difference between the neutron and proton potentials in Eqs. (21) and (25), and the effective mass in Eqs. (19) and (24). The relationship of a_4 with δR, however, does not seem to be described explicitly. In fact, there is more a fundamental restriction on the relationship between the potential and the effective mass. It is known as the Hugenholtz–Van Hove (HVH) theorem [19–21], which holds in any mean-field model for symmetric nuclear matter.

4. Hugenholtz–Van Hove theorem

According to the HVH theorem, the binding energy per nucleon is equal to the Fermi energy in symmetric nuclear matter. Both relativistic and non-relativistic models have been constructed so as to satisfy the theorem at values of the binding energy of the nucleon of about -16 MeV and of the Fermi momentum of about 1.3 fm^{-1}. These values are used as inputs in order to fix their free parameters in the nuclear interactions. The Fermi energy is given by the sum of the kinetic and potential energy, so that the strength of the potential and the value of the effective mass are constrained by these inputs. Since the HVH theorem has only been proved for symmetric

Downloaded from https://academic.oup.com/ptep/article/2022/2/023D03/6507566 by Deutsches Elektronen Synchrotron DESY user on 23 March 2022

nuclear matter [19–21], however, we will extend the theorem to relativistic and non-relativistic asymmetric nuclear matter and utilize the theorem as a guide to the analysis of δR in neutron-rich finite nuclei.

4.1 *HVH theorem in symmetric nuclear matter*

Hugenholtz and Van Hove have shown that the following equation holds in the non-relativistic mean-field model for symmetric nuclear matter [19–21]:

$$\frac{\varepsilon}{\rho} = E_{\rm F}, \quad \text{when} \quad \frac{d}{d\rho}\frac{\varepsilon}{\rho} = 0, \tag{29}$$

where ε stands for the total energy density of the system and $E_{\rm F}$ the Fermi energy. The value of ε/ρ represents the binding energy per nucleon, $E_{\rm B}$, to be written in the non-relativistic models, as

$$E_{\rm B} = E_{\rm F} = \frac{k_{\rm F}^2}{2m^* M} + V. \tag{30}$$

In the relativistic models, ε/ρ and $E_{\rm F}$ contain the nucleon rest mass. Hence, $E_{\rm B}$ and $E_{\rm F}$ are given by

$$E_{\rm B} = \frac{\varepsilon}{\rho} - M = E_{\rm F} - M\,.$$

In the present relativistic models, $E_{\rm F}$ in the symmetric nuclear matter is written as [14]

$$E_{\rm F} = \sqrt{k_{\rm F}^2 + M_\sigma^2} + V_\omega, \qquad M_\sigma = M + V_\sigma.$$

In setting

$$E_{\rm B} = K + V, \quad K = \sqrt{k_{\rm F}^2 + M_\sigma^2} - M_\sigma, \quad V = V_\sigma + V_\omega,$$

K is described as

$$K = \frac{k_{\rm F}^2}{2M^*}(1-\delta) \approx \frac{k_{\rm F}^2}{2M^*}, \tag{31}$$

with $M^* = M + (V_\sigma - V_\omega)/2$ from Eq. (22). We have defined

$$\delta = 1 - \frac{2M^*}{k_{\rm F}^2}\left(\sqrt{k_{\rm F}^2 + M_\sigma^2} - M_\sigma\right), \tag{32}$$

and used the fact that $\delta \ll 1$ in taking the values of Ref. [22] for the right-hand side. Thus, in the relativistic models also, $E_{\rm B}$ is expressed in the form of Eq. (30). Finally, in both relativistic and non-relativistic models, the nuclear potential is inversely proportional to the effective mass, according to the HVH theorem. In the case of Eq. (30), we have

$$V = \frac{a}{m^*} + b, \tag{33}$$

where $a \approx -35$ MeV and $b \approx -16$ MeV for $k_{\rm F} \approx 1.3$ fm^{-1} and $E_{\rm B} \approx -16$ MeV.

Indeed, it is verified that all the relativistic and non-relativistic models employed in the present paper satisfy Eq. (29) explicitly. In the non-relativistic models, we have for the protons and neutrons, separately,

$$\frac{\partial \varepsilon}{\partial \rho_\tau} = \frac{k_{{\rm F}\tau}^2}{2M_\tau^*} + V_\tau = E_{{\rm F}\tau}, \tag{34}$$

while, in the relativistic σ–ω–ρ models,

$$\frac{\partial \varepsilon}{\partial \rho_\tau} = \sqrt{k_{{\rm F}\tau}^2 + M_\sigma^2} + V_\omega + \tau V_\rho = E_{{\rm F}\tau}. \tag{35}$$

Downloaded from https://academic.oup.com/ptep/article/2022/2/023D03/6507566 by Deutsches Elektronen Synchrotron DESY user on 23 March 2022

In the above equations, the total energy density in the non-relativistic models is written as [23,24]

$$\varepsilon = \frac{K_p}{2M_p^*} + \frac{K_n}{2M_n^*} + \frac{t_0}{4}\big((2+x_0)\rho^2 - (2x_0+1)\big(\rho_p^2+\rho_n^2\big)\big)$$
$$+ \frac{t_3}{24}\big((2+x_3)\rho^{\alpha+2} - (2x_3+1)\rho^{\alpha}\big(\rho_p^2+\rho_n^2\big)\big),$$

where we have defined $K_\tau = 3k_{\mathrm{F}\tau}^2\rho_\tau/5$ with $k_{\mathrm{F}\tau} = (3\pi^2\rho_\tau)^{1/3}$. In the relativistic models, it is given by

$$\varepsilon = \varepsilon_K + V_\omega\rho + V_\rho(\rho_p - \rho_n) + U_\sigma - U_0,$$

using the abbreviations

$$\varepsilon_K = \frac{2}{(2\pi)^3}\int_0^{k_{\mathrm{F}p}} d^3k\sqrt{k^2+M_\sigma^2} + \frac{2}{(2\pi)^3}\int_0^{k_{\mathrm{F}n}} d^3k\sqrt{k^2+M_\sigma^2},$$

$$U_\sigma = \frac{m_\sigma^2}{2g_\sigma^2}V_\sigma^2 + \frac{g_3}{3g_\sigma^3}V_\sigma^3 + \frac{g_4}{4g_\sigma^4}V_\sigma^4, \qquad U_0 = \frac{m_\omega^2}{2g_\omega^2}V_\omega^2 + \frac{c_4}{4g_\omega^4}V_\omega^4 + \frac{m_\rho^2}{2g_\rho^2}V_\rho^2 + \lambda V_\omega^2 V_\rho^2, \quad (36)$$

which satisfy the equations of motion for the mesons:

$$\frac{\partial U_\sigma}{\partial V_\sigma} = \frac{m_\sigma^2}{g_\sigma^2}V_\sigma + \frac{g_3}{g_\sigma^3}V_\sigma^2 + \frac{g_4}{g_\sigma^4}V_\sigma^3 = -\rho_S, \qquad \rho_S = \frac{\partial\varepsilon_K}{\partial M_\sigma},$$

$$\frac{\partial U_0}{\partial V_\omega} = \frac{m_\omega^2}{g_\omega^2}V_\omega + \frac{c_4}{g_\omega^4}V_\omega^3 + 2\lambda V_\omega V_\rho^2 = \rho\,, \qquad \frac{\partial U_0}{\partial V_\rho} = \frac{m_\rho^2}{g_\rho^2}V_\rho + 2\lambda V_\omega^2 V_\rho = \rho_p - \rho_n.$$

In both relativistic and non-relativistic models, $\partial\varepsilon/\partial\rho_\tau = E_{\mathrm{F}\tau}$ holds at any value of ρ or k_{F}, so that we have, for $\rho_p = \rho_n = \rho/2$,

$$\frac{d\varepsilon}{d\rho} = \frac{1}{2}\left(\frac{\partial\varepsilon}{\partial\rho_p} + \frac{\partial\varepsilon}{\partial\rho_n}\right) = \frac{E_{\mathrm{F}n}+E_{\mathrm{F}n}}{2} = E_{\mathrm{F}}, \qquad \rho\frac{d}{d\rho}\frac{\varepsilon}{\rho} = \frac{d\varepsilon}{d\rho} - \frac{\varepsilon}{\rho} = E_{\mathrm{F}} - \frac{\varepsilon}{\rho},$$

as we should. The last equation yields Eq. (29) for $(d/d\rho)(\varepsilon/\rho) = 0$. Thus, in the mean-field models, Eqs. (34) and (35), which hold for protons and neutrons separately, are essential for the HVH theorem to be valid.

4.2 *HVH theorem in asymmetric nuclear matter*

In order to discuss neutron-rich nuclei using the HVH theorem as a guide, we have to extend the theorem so as to be applicable to relativistic and non-relativistic asymmetric nuclear matter.

One of the naive ways to do this may be to minimize the total energy per nucleon, assuming $\rho_n = \nu\rho$ and $\rho_p = (1-\nu)\rho$ for a fixed value of ν [1,13,24]. This choice is not, however, appropriate for the present purpose, since $E_{\mathrm{F}n}$ and $E_{\mathrm{F}p}$ remain as in Eqs. (34) and (35) without the Coulomb energy. Moreover, if $\rho_n(r) = \nu\rho(r)$ and $\rho_p(r) = (1-\nu)\rho(r)$ were realized in finite nuclei, one would have $\delta R = 0$ even for $N \neq Z$ nuclei. In order to extend the HVH theorem for asymmetric nuclear matter, it is be better to avoid these defects. For this purpose, without using the parameter ν, we make a model for the neutron and proton system taking into account the effects of the "Coulomb potential" explicitly, as below.

We require, for asymmetric nuclear matter,

$$\frac{\partial}{\partial\rho_\tau}\frac{\varepsilon_{\mathrm{asym}}}{\rho} = 0, \quad (37)$$

adding $v_c\rho_p$ as the "Coulomb term" to the total energy density [27],

$$\varepsilon_{\mathrm{asym}} = \varepsilon + v_c\rho_p, \quad (38)$$

Downloaded from https://academic.oup.com/ptep/article/2022/2/023D03/6507566 by Deutsches Elektronen Synchrotron DESY user on 23 March 2022

where v_c is a constant. The above equation is assumed in order to make a model that may be used just as a guide for the following discussions on the stable finite nucleus where the Fermi energies of neutrons and protons are the same and the Coulomb potential is necessary. We will see later that the final results of this paper listed in Table 12 do not depend on the above form of the "Coulomb term" and its strength v_c. Then, since Eqs. (34) and (35) still hold, we have the expression for the binding energy,

$$E_{\rm B} = E_{{\rm F}\tau} = \frac{k_{{\rm F}\tau}^2}{2M_\tau^*} + V_\tau + \frac{1+\tau_3}{2} v_c, \tag{39}$$

in the non-relativistic models, while, in the relativistic models,

$$\begin{aligned} E_{\rm B} = E_{{\rm F}\tau} - M &= \sqrt{k_{{\rm F}\tau}^2 + M_\sigma^2} - M_\sigma + V_\tau + \frac{1+\tau_3}{2} v_c \\ &= (1-\delta_\tau)\frac{k_{{\rm F}\tau}^2}{2M_\tau^*} + V_\tau + \frac{1+\tau_3}{2} v_c, \end{aligned} \tag{40}$$

where δ_τ is given by Eq. (32) with $k_{{\rm F}\tau}$ and M_τ^* instead of $k_{\rm F}$ and M^*, respectively, while V_τ and M_τ^* are given by Eqs. (21) and (22). The Coulomb potential in Eq. (22) is neglected here, since its role is expected to be small, compared to that from $(V_\sigma(\boldsymbol{r}) - V_\omega(\boldsymbol{r}) - V_\rho(\boldsymbol{r}))$ in Eq. (22). The value of $(V_\sigma(\boldsymbol{r}) - V_\omega(\boldsymbol{r}) - V_\rho(\boldsymbol{r}))$ at $r = 0$ is about -680 MeV, as noted below Eq. (22). Equations (39) and (40) are accepted as the HVH theorem in asymmetric nuclear matter, and imply a relationship between V_τ and m_τ^* as in Eq. (33),

$$V_\tau = \frac{a_\tau}{m_\tau^*} + b_\tau, \qquad a_\tau = -(1-\delta_\tau)\frac{k_{{\rm F}\tau}^2}{2M}, \qquad b_\tau = \begin{cases} E_{\rm B}, & \tau = n \\ E_{\rm B} - v_c, & \tau = p, \end{cases} \tag{41}$$

where $\delta_\tau = 0$ in the non-relativistic models, while in the relativistic models $|\delta_\tau| \ll 1$ is almost constant. The values of $k_{{\rm F}\tau}^2$, which provide the values of ρ_τ in the relativistic and non-relativistic models, are determined by the two equations in Eq. (37), once v_c is given by hand.

For simplicity, for both relativistic and non-relativistic models, we take v_c from the strength at $r = 0$ of the Coulomb potential for a uniformly charged sphere of radius $r_c A^{1/3}$:

$$v_c = \frac{3}{2}\frac{Z\alpha}{r_c A^{1/3}}. \tag{42}$$

This yields $v_c = 22.144$ MeV for ^{208}Pb with $r_c = 1.350$ fm. In employing this value, we obtain Fig. 1 for the $1/m_\tau^*$–V_τ relationship corresponding to Eq. (41). The black circles indicate the values from the 11 relativistic models, the red ones those from the 9 non-relativistic models. These models have been employed in Ref. [4]. Each circle is accompanied by a number that shows the model used. The numbering is according to Ref. [4]: 1.L2 [15], 2.NLB [15], 3.NLC [15], 4.NL1 [28], 5.NL3 [22], 6.NL-SH [29], 7.NL-Z [30], 8.NL-S [31], 9.NL3II [22], 10.TM1 [32], and 11.FSU [16] for the relativistic nuclear models, and 1.SKI [25], 2.SKII [25], 3.SKIII [33], 4.SKIV [33], 5.SkM* [34], 6.SLy4 [24], 7.T6 [35], 8.SGII [36], and 9.Ska [37] for the non-relativistic models. This numbering will be used throughout the present paper.

In Fig. 1, the least-square lines (LSLs) of these circles are shown by black ones for the relativistic models and red ones for the non-relativistic models. The LSLs for neutrons and protons are well separated from each other in both the relativistic and non-relativistic models. The effective mass and the one-body potential are complicated functions of the interaction parameters whose values are different from one another between the mean-field models. Nevertheless, as seen in Fig. 1, all the circles are almost on their own LSLs.

Downloaded from https://academic.oup.com/ptep/article/2022/2/023D03/6507566 by Deutsches Elektronen Synchrotron DESY user on 23 March 2022

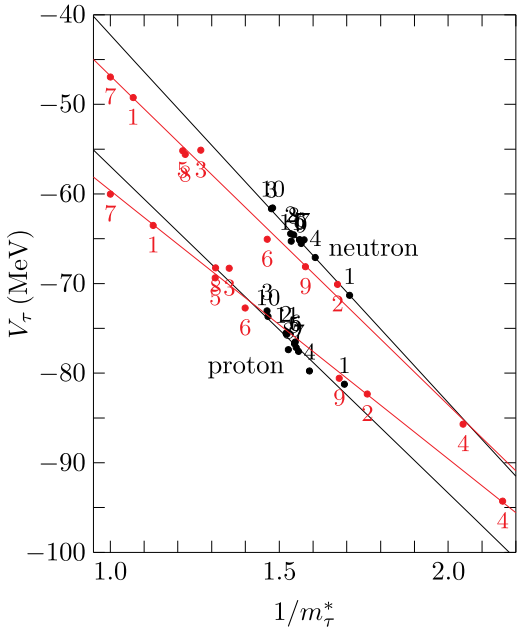

Fig. 1. The relationship between the effective mass and the one-body potential for neutrons ($\tau = n$) and protons ($\tau = p$) in the mean-field models for asymmetric nuclear matter. The black circles show the values calculated by the 11 relativistic models, while the red ones show those by the 9 non-relativistic models. Each circle is accompanied by a number that indicates the model used, specified in the text. The least-square lines are shown for the four groups. The two black lines are obtained from the black circles for neutrons and protons, respectively, and the red lines from the red circles.

On the one hand, the circle at $(m^*_{\tau,i}, V_{\tau,i})$ of model i is given by

$$V_{\tau,i} = a_{\tau,i}/m^*_{\tau,i} + b_{\tau,i}, \tag{43}$$

according to Eq. (41) by the HVH theorem. On the other hand, the LSL satisfies

$$V^{\rm L}_{\tau,i} = a^{\rm L}_\tau/m^*_{\tau,i} + b^{\rm L}_\tau, \tag{44}$$

where $a^{\rm L}_\tau$ and $b^{\rm L}_\tau$ denote the slope and intercept of the LSL, respectively. In writing the average value of Eq. (43) as $\langle V_{\tau,i}\rangle$ and that of Eq. (44) as $\langle V^{\rm L}_{\tau,i}\rangle$, they are equal to each other by the definition of the LSL, $\langle V_{\tau,i}\rangle = \langle V^{\rm L}_{\tau,i}\rangle$, yielding

$$\langle a_{\tau,i}/m^*_{\tau,i}\rangle + \langle b_{\tau,i}\rangle = a^{\rm L}_\tau\langle 1/m^*_{\tau,i}\rangle + b^{\rm L}_\tau. \tag{45}$$

Hence, if the following approximation is valid,

$$\langle a_{\tau,i}/m^*_{\tau,i}\rangle \approx \langle a_{\tau,i}\rangle/\langle m^*_{\tau,i}\rangle, \quad \langle 1/m^*_{\tau,i}\rangle \approx 1/\langle m^*_{\tau,i}\rangle, \tag{46}$$

then we have

$$\langle m^*_\tau\rangle\langle V_\tau\rangle \approx \langle a_\tau\rangle + \langle b_\tau\rangle\langle m^*_\tau\rangle \approx a^{\rm L}_\tau + b^{\rm L}_\tau\langle m^*_\tau\rangle \tag{47}$$

by writing $\langle V_{\tau,i}\rangle = \langle V_\tau\rangle$, $\langle a_{\tau,i}\rangle = \langle a_\tau\rangle$, $\langle b_{\tau,i}\rangle = \langle b_\tau\rangle$, and $\langle m^*_{\tau,i}\rangle = \langle m^*_\tau\rangle$.

In Table 2 are listed the values of the slope $a^{\rm L}_\tau$ and intercept $b^{\rm L}_\tau$ of the LSL. The average values of $a_{\tau,i}$ and $b_{\tau,i}$ calculated by each model are tabulated as $\langle a_\tau\rangle$ and $\langle b_\tau\rangle$. The average values of the effective mass $\langle m^*_\tau\rangle$ and of the strengths of the one-body potentials $\langle V_\tau\rangle$ are also listed, together with the average values of $\rho_{\tau,i}$ as $\langle\rho_\tau\rangle$.

The difference between the values of $\langle a_\tau\rangle$ in the relativistic and non-relativistic models is related to those of $\langle\rho_\tau\rangle$ through the Fermi momentum. The values of $\langle b_\tau\rangle$ are almost the same

Downloaded from https://academic.oup.com/ptep/article/2022/2/023D03/6507566 by Deutsches Elektronen Synchrotron DESY user on 23 March 2022

Table 2. The values of the gradient ($a_\tau^{\rm L}$) and the intercept ($b_\tau^{\rm L}$) of the least-square lines in units of MeV for the relationship between $1/m_\tau^*$ and V_τ in Fig. 1. The average values of the coefficients in Eq. (43) are also listed as $\langle a_\tau\rangle$ and $\langle b_\tau\rangle$, together with those of the effective masses, the strengths of the one-body potentials (MeV), and the nuclear matter densities (fm^{-3}) in the relativistic (Rel) and non-relativistic (Non) models. The notations of n and p indicate that the values in the corresponding rows are for neutrons and protons, respectively. For details, see the text.

		$a_\tau^{\rm L}$	$b_\tau^{\rm L}$	$\langle a_\tau\rangle$	$\langle b_\tau\rangle$	$\langle m_\tau^*\rangle$	$\langle V_\tau\rangle$	$\langle\rho_\tau\rangle$
Rel	n	− 41.059	− 1.176	− 38.011	− 5.918	0.6426	− 65.160	0.0832
	p	− 36.489	− 20.421	− 31.530	− 28.063	0.6488	− 76.742	0.0611
Non	n	− 36.743	− 10.069	− 39.927	− 5.840	0.7524	− 61.219	0.0903
	p	− 29.960	− 29.656	− 31.168	− 27.984	0.7217	− 73.256	0.0623

Table 3. The product of the mean values of the effective mass $\langle m_\tau^*\rangle$ and the one-body potential $\langle V_\tau\rangle$. The numbers are given in units of MeV. For details, see the text.

		$\langle m_\tau^*\rangle\langle V_\tau\rangle$	$a_\tau^{\rm L}+b_\tau^{\rm L}\langle m_\tau^*\rangle$	$\langle a_\tau\rangle+\langle b_\tau\rangle\langle m_\tau^*\rangle$
Rel	n	−41.872	−41.815	−41.814
	p	−49.790	−49.738	−49.737
Non	n	−46.061	−44.319	−44.321
	p	−52.869	−51.363	−51.364

between the two frameworks, since $\langle b_\tau\rangle$ satisfies the relationships $\langle E_{\rm B}\rangle = \langle b_n\rangle$ and $v_c = \langle b_n\rangle - \langle b_p\rangle$, where $\langle E_{\rm B}\rangle$ denotes the average value of $E_{{\rm B},i}$, according to Eq. (41).

The values of $a_\tau^{\rm L}$ and $b_\tau^{\rm L}$ depend on the distributions of the points ($m_{\tau,i}^*$, $V_{\tau,i}$) and have no simple relationship with $\langle\rho_\tau\rangle$, $\langle E_{\rm B}\rangle$, and v_c. They, however, are implicitly constrained by the HVH theorem through Eq. (47). Since the values of v_c and $\langle E_{\rm B}\rangle$ are almost the same in the relativistic and non-relativistic models, Eq. (47) provides the relationship between the effective mass, the strength of the one-body potential, and the nucleon density. This fact implies that the LSL coefficients $a_\tau^{\rm L}$ and $b_\tau^{\rm L}$ are dominated by $\langle\rho_\tau\rangle$ implicitly.

Equation (47) is rewritten as $a_\tau^{\rm L} - \langle a_\tau\rangle \approx (\langle b_\tau\rangle - b_\tau^{\rm L})\langle m_\tau^*\rangle$, which provides the relationship $a_\tau^{\rm L} \gtrsim \langle a_\tau\rangle$ for $b_\tau^{\rm L} \lesssim \langle b_\tau\rangle$, and $a_\tau^{\rm L} \lesssim \langle a_\tau\rangle$ for $b_\tau^{\rm L} \gtrsim \langle b_\tau\rangle$. The non-relativistic models obey the first case, the relativistic ones the second case. The value of $|b_n^{\rm L}|$ is made much smaller by the small $\langle m_n^*\rangle$ in the relativistic models, compared to that in the non-relativistic ones.

In Table 3, the value of each term in Eq. (47) is listed. It shows that the values of $\langle m_\tau^*\rangle\langle V_\tau\rangle$ are a little larger than those of $\langle a_\tau\rangle + \langle b_\tau\rangle\langle m_\tau^*\rangle$ and $a_\tau^{\rm L} + b_\tau^{\rm L}\langle m_\tau^*\rangle$ in the non-relativistic models, because the approximations in Eq. (46) are a little worse in the non-relativistic models than in the relativistic models. This difference, however, is not essential for the present discussions on δR.

In finite nuclei, Eq. (9) indicates that the radius depends on $(-\langle m_\tau^*\rangle\langle V_\tau\rangle)^{-1/4}$. Table 3 implies a possibility that R_n is larger in the relativistic models than in the non-relativistic ones, if the same tendency maintains in finite nuclei. In the mean-field models for finite nuclei, however, the effective mass and one-body potential may have complicated coordinate dependences. In order to confirm the above implications for finite nuclei, we need a way to extract from them the values of the effective mass and the strength of the one-body potentials that are appropriate for use in Eq. (9). Moreover, it is desirable to explore whether or not they are constrained by

Downloaded from https://academic.oup.com/ptep/article/2022/2/023D03/6507566 by Deutsches Elektronen Synchrotron DESY user on 23 March 2022

the HVH theorem as in asymmetric nuclear matter. Although we do not have for finite nuclei an equation like Eq. (37) to yield the HVH constraint in asymmetric nuclear matter, Eq. (47) may be helpful for understanding the roles of the HVH theorem in finite nuclei. Bearing these facts in mind, we proceed to discuss finite nuclei from the next section.

5. Simplification of the mean-field models

One of the ways to find a common structure of the models is to simplify them without losing their main characteristics. By defining the effective mass and the one-body potential in such a way, we may find their relationships with R and a restriction between them like the HVH lines, which are hidden in the complexity of the calculated results of the mean-field models for finite nuclei.

In this section, we will analyze the structure of the relativistic and non-relativistic models by simplifying their descriptions as much as possible. As mentioned in Section 3, R_τ may be a functional of $V_\tau(r)$, $M^*_\tau(r)$, $V_c(r)$, and the spin–orbit potential, $V_{\ell s,\tau}(r)$, but among them, it is expected that $V_c(r)$ and $V_{\ell s,\tau}(r)$ play a minor role in the difference between δR in the two frameworks, $\delta R[V_\tau, M^*_\tau, V_c, V_{\ell s,\tau}] \approx \delta R[V_\tau, M^*_\tau]$. Using these facts as a guide, let us express approximately all the Hamiltonians in both frameworks, using the same basis.

5.1 *Nuclear potential and effective mass*

The fundamental properties of nuclei are well described with the WS potential [1], and its structure is clear for the present purpose to discuss δR, as in Eq. (10). Hence, we approximate the mean-field potential, $V_\tau(r)$, and the effective mass, $M^*_\tau(r)$, in both frameworks by using the WS-type function,

$$f_\tau(r) = f_\tau(r, R_\tau, a_\tau) = \frac{1}{1+\exp((r-R_\tau)/a_\tau)}, \tag{48}$$

i.e.,

$$V_\tau(r) \approx V_{\mathrm{ws},\tau} f(r, R_{\mathrm{ws},\tau}, a_{\mathrm{ws},\tau}), \tag{49}$$

$$m^*_\tau(r) \approx \begin{cases} 1 + \left(m^*_{\mathrm{ws},\tau} - 1\right) f\left(r, R^*_{\mathrm{ws},\tau}, a^*_{\mathrm{ws},\tau}\right) - \frac{V_c(r)}{2M}\frac{1+\tau_3}{2}, & \text{(Rel)}, \\ 1 + \left(m^*_{\mathrm{ws},\tau} - 1\right) f\left(r, R^*_{\mathrm{ws},\tau}, a^*_{\mathrm{ws},\tau}\right), & \text{(Non)}, \end{cases} \tag{50}$$

where $m^*_\tau(r) = M^*_\tau(r)/M$ is defined, and Rel and Non indicate the relativistic and non-relativistic models, respectively. The three parameters on the right-hand sides of the above equations are determined by minimizing, e.g., for $V_\tau(r)$, the following quantity with respect to $V_{\mathrm{ws},\tau}$, $R_{\mathrm{ws},\tau}$, and $a_{\mathrm{ws},\tau}$:

$$\int_0^\infty dr\, r^2 (V_\tau(r) - V_{\mathrm{ws},\tau} f(r, R_{\mathrm{ws},\tau}, a_{\mathrm{ws},\tau}))^2. \tag{51}$$

Here, the volume integral has been chosen in order to minimize the above deviation, since both $V_\tau(r)$ and $V_{\mathrm{ws},\tau} f(r, R_{\mathrm{ws},\tau}, a_{\mathrm{ws},\tau})$ are expected to have a similar shape to that of the nuclear density whose volume integral value is constrained by the nucleon number. In deriving Eq. (9), we have used $n = 0$ in Eq. (4), since there is not such a constraint on the HO potential, but since it is important to keep the similarity of the wave functions in the HO and WS potentials.

Downloaded from https://academic.oup.com/ptep/article/2022/2/023D03/6507566 by Deutsches Elektronen Synchrotron DESY user on 23 March 2022

5.2 *Coulomb potential*

In the relativistic models, the Coulomb energy is calculated by taking into account the only direct term of the interaction in the same way as for other interactions, while the exchange term is also included in the non-relativistic models. The Coulomb interaction, however, plays a minor role in the present purpose on δR, so that we simply express it by that of the uniform charge distribution with the radius, $R_{\rm coul}$:

$$V_c(r) \approx V_{\rm sph}(r), \qquad V_{\rm sph}(r) = \begin{cases} \dfrac{Z\alpha}{2R_{\rm coul}}\left(3 - \dfrac{r^2}{R_{\rm coul}^2}\right), & r < R_{\rm coul}, \\ \dfrac{Z\alpha}{r}, & r > R_{\rm coul}. \end{cases} \tag{52}$$

The radius $R_{\rm coul}$ is determined by minimizing the deviation:

$$\int_0^\infty dr\, r^2 (V_c(r) - V_{\rm sph}(r))^2.$$

The value of $R_{\rm coul}$ of each model will be shown later.

5.3 *Spin–orbit potential*

We express the spin–orbit potential in the form:

$$V_{\ell s,\tau}(r) = V_{\ell s,\tau} \frac{1}{r}\frac{df_\tau(r)}{dr} \boldsymbol{\ell}\cdot\boldsymbol{\sigma}. \tag{53}$$

In the relativistic models, it is written from Eq. (20) as

$$\begin{aligned} V_{\ell s,\tau}(r) &= \frac{1}{r}\frac{d}{dr}\frac{1}{2M_\tau^*(r)}\boldsymbol{\ell}\cdot\boldsymbol{\sigma} = -\frac{1}{2M}\frac{1}{m_\tau^{*2}(r)}\frac{1}{r}\frac{dm_\tau^*(r)}{dr}\boldsymbol{\ell}\cdot\boldsymbol{\sigma} \\ &\approx \frac{1 - m_{{\rm ws},\tau}^*}{2M}\frac{1}{m_\tau^{*2}(r)}\frac{1}{r}\frac{d}{dr} f\left(r, R_{{\rm ws},\tau}^*, a_{{\rm ws},\tau}^*\right)\boldsymbol{\ell}\cdot\boldsymbol{\sigma}, \end{aligned} \tag{54}$$

neglecting $V_c(r)$ in Eq. (50). In the calculations, a further approximation has been used, $m_\tau^*(r) \approx m_\tau^*(R_{{\rm ws},\tau}^*) = (1 + m_{{\rm ws},\tau}^*)/2$.

In the non-relativistic models, the spin–orbit potential of Eq. (26) is approximated as

$$V_{\ell s,\tau}(r) = \frac{W_0}{2r}\frac{d}{dr}(\rho(r) + \rho_\tau(r))\boldsymbol{\ell}\cdot\boldsymbol{\sigma} \approx \frac{W_0\rho_0}{2}\left(1 + \frac{N_\tau}{A}\right)\frac{1}{r}\frac{d}{dr} f(r, R_{\rm den}, a_{\rm den})\,\boldsymbol{\ell}\cdot\boldsymbol{\sigma}, \tag{55}$$

where the value of W_0 is fixed at 120 MeV fm^5 and we have written the nuclear density as

$$\rho(r) = \rho_p(r) + \rho_n(r) \approx \rho_0 f(r, R_{\rm den}, a_{\rm den}),$$

with

$$4\pi\rho_0 \int_0^\infty dr\, r^2 f(r, R_{\rm den}, a_{\rm den}) = A.$$

The details of the calculation of the nuclear density will be mentioned in Section 5.6.

In fact, the spin–orbit potentials are expected not to play an important role in understanding the difference of δR between the relativistic and non-relativistic models, since their strengths are similar and the isospin dependences are small, in addition to the reason mentioned before.

5.4 *A few examples*

Before summarizing the results of the present section, let us compare $V_\tau(r)$, $\rho_\tau(r)$, and $m_\tau^*(r)$ from the exact mean-field calculations with those of the corresponding simplified Hamiltonian, by taking a few examples. After minimizing Eq. (51), the only values of $V_{{\rm ws},n}$ for the relativistic WS potentials have been multiplied by 0.99, so as to reproduce well the values of R_n in the

Downloaded from https://academic.oup.com/ptep/article/2022/2/023D03/6507566 by Deutsches Elektronen Synchrotron DESY user on 23 March 2022

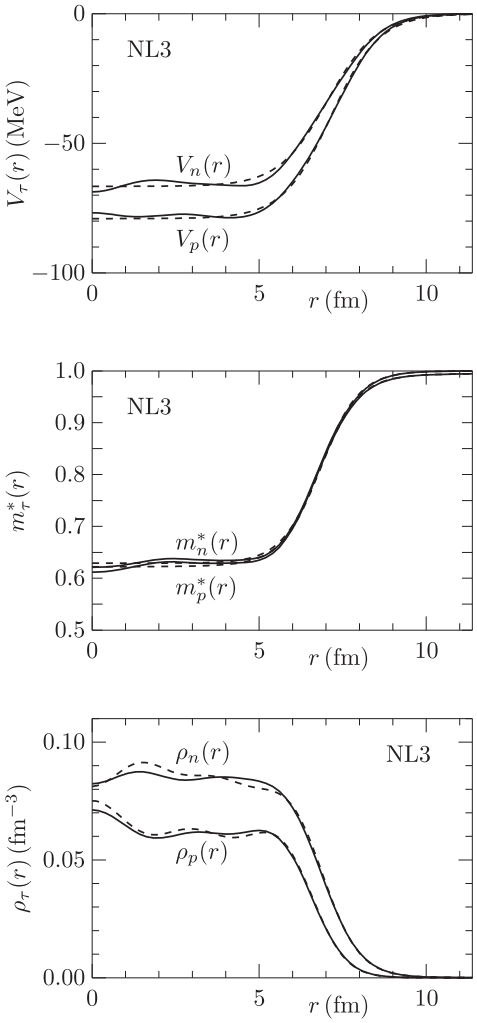

Fig. 2. The one-body potentials, the effective masses, and the densities for neutrons ($\tau = n$) and protons ($\tau = p$) in ^{208}Pb. The solid curves are obtained by the relativistic mean-field model with NL3, the dashed ones by its simplified Hamiltonian.

exact relativistic mean-field calculations. This factor makes the mean value of R_n from the WS potential smaller by about 0.015 fm.

Fig. 2 shows the results of the one-body potentials, the effective masses, and the neutron and proton densities for ^{208}Pb calculated with NL3. The solid curves are obtained by full calculations, the dashed ones by simplified Hamiltonians. All other relativistic models yield similar results. In non-relativistic models, we show the results for SkM* in Fig. 3. These results of SKM* are similar to those of other models except for the effective mass in SLy4. In SLy4, the coordinate dependences of the effective mass are similar to those in Fig. 3, but the relation of the magnitude between $m^*_{\mathrm{ws},p}$ and $m^*_{\mathrm{ws},n}$ is opposite to that in other non-relativistic models. It is seen that all the results using simplified versions well reproduce the corresponding ones obtained with full calculations.

5.5 *Results using the simplified models*

Table 4 shows the root msrs of the point neutron distributions in ^{48}Ca and ^{208}Pb determined in Ref. [4]. Those of the point proton distributions obtained in a similar way are also listed.

Downloaded from https://academic.oup.com/ptep/article/2022/2/023D03/6507566 by Deutsches Elektronen Synchrotron DESY user on 23 March 2022

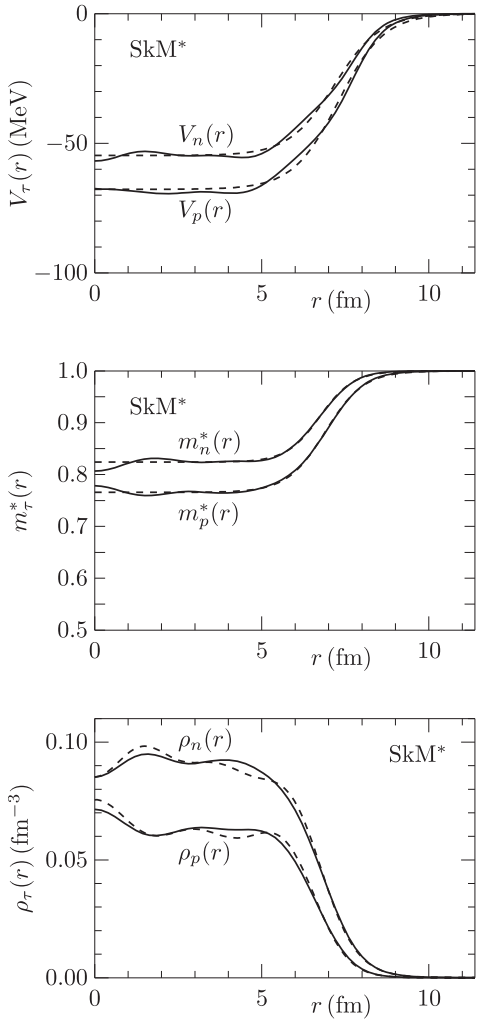

Fig. 3. The one-body potentials, the effective masses, and the densities for neutrons ($\tau = n$) and protons ($\tau = p$) in ^{208}Pb. The solid curves are obtained by the non-relativistic mean-field model with SkM*, the dashed ones by its simplified Hamiltonian.

Table 4. The results of the least-squares analysis in Ref. [4]. The numbers in the parentheses denote the error that is obtained taking account of the experimental error and the standard deviation of the calculated values from the least-square line. All the numbers are given in units of fm. For details, see the text.

		R_n	R_p	δR
	Rel	3.597(0.021)	3.378(0.005)	0.220(0.026)
^{48}Ca	Non	3.492(0.028)	3.372(0.009)	0.121(0.036)
	Rel	5.728(0.057)	5.454(0.013)	0.275(0.070)
^{208}Pb	Non	5.609(0.054)	5.447(0.014)	0.162(0.068)

The errors in the parentheses are given by taking into account the experimental error and the standard deviation of the LSL. Since both relativistic and non-relativistic models employ experimental values of the msrs of the nuclear charge distributions as an input, the values of R_p in the two frameworks are almost equal to each other, while the values of R_n are larger by about

Downloaded from https://academic.oup.com/ptep/article/2022/2/023D03/6507566 by Deutsches Elektronen Synchrotron DESY user on 23 March 2022

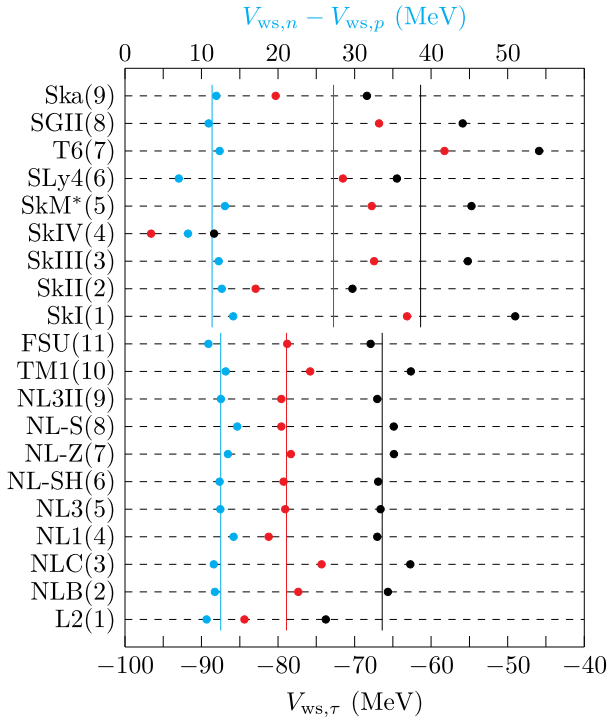

Fig. 4. The strength of the one-body potentials for neutrons ($\tau = n$) and protons ($\tau = p$) in ^{208}Pb. On the left-hand side, the relativistic and non-relativistic models are indicated. The black circles represent the strengths of the neutron potentials, the red ones those of the proton potentials, and the blue ones the differences between their two strengths. The vertical lines stand for the average values of the corresponding circles in the relativistic and non-relativistic models, separately. The scale along the bottom shows the strengths of the potentials, that along the top the difference between the strengths of the neutron and proton potentials.

0.1 fm in the relativistic models than in the non-relativistic ones in both ^{48}Ca and ^{208}Pb. The purpose of the present paper is to understand this difference between R_n.

We note that the new data from JLab have been reported in Ref. [5], according to the parity-violating electron scattering experiment. These provide δR in ^{208}Pb as 0.283 ± 0.071 fm. This is almost the same as the value of δR in Table 3 in the relativistic models, and is not incompatible with the non-relativistic one taking into account their errors. The analysis of the JLab data [5] is model dependent as in Ref. [4], and Ref. [38] has obtained $\delta R = 0.19 \pm 0.02$ fm from the JLab data on the basis of the different model analyses.

Let us summarize the results in the present section for ^{208}Pb. Fig. 4 shows the values of $V_{\mathrm{ws},\tau}$ in Eq. (49) for the relativistic and non-relativistic models. The strengths of the neutron potentials are shown by the black circles, those of the proton ones by the red circles. It is seen that the non-relativistic ones are distributed over a wide range, as expected, in contrast to those of relativistic models. The straight vertical lines show their average values. The difference between $V_{\mathrm{ws},n} - V_{\mathrm{ws},p}$, however, is almost equal, independent of the models, as shown by the blue circles and the straight lines indicating their average values. Thus, the difference is only a little larger in the relativistic models than in the non-relativistic ones. This fact implies that the difference between δR in the two frameworks may not be due to the symmetry potentials only.

Fig. 5 shows the values of $R_{\mathrm{ws},\tau}$ in a similar way to Fig. 4. The black and red circles for the non-relativistic models are again distributed over a wide region, compared to those of the

Downloaded from https://academic.oup.com/ptep/article/2022/2/023D03/6507566 by Deutsches Elektronen Synchrotron DESY user on 23 March 2022

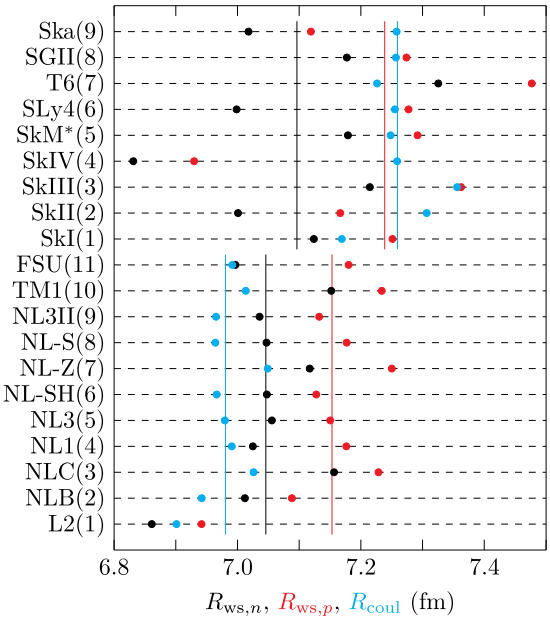

Fig. 5. The radius parameters of the Woods–Saxon potentials for neutrons ($\tau = n$) and protons ($\tau = p$) in ^{208}Pb obtained from the relativistic and non-relativistic mean-field models. On the left-hand side, the relativistic and non-relativistic models used are indicated. The black circles represent the values of the radius parameter $R_{\mathrm{ws},n}$, the red ones those of $R_{\mathrm{ws},p}$. The blue ones stand for the values of the radius parameters of the Coulomb potentials. The vertical lines indicate the average values of the corresponding circles in the relativistic and non-relativistic models, separately.

Table 5. The mean values of the Woods–Saxon parameters, the strengths of the one-body potentials, and the effective masses in the relativistic and non-relativistic models. The numbers of $\langle R_{\mathrm{ws},\tau}\rangle$ and $\langle a_{\mathrm{ws},\tau}\rangle$ are given in units of fm, those of $\langle V_{\mathrm{ws},\tau}\rangle$ in units of MeV. For details, see the text.

	$\langle R_{\mathrm{ws},n}\rangle$	$\langle R_{\mathrm{ws},p}\rangle$	$\langle a_{\mathrm{ws},n}\rangle$	$\langle a_{\mathrm{ws},p}\rangle$	$\langle V_{\mathrm{ws},n}\rangle$	$\langle V_{\mathrm{ws},p}\rangle$	$\langle m^*_{\mathrm{ws},n}\rangle$	$\langle m^*_{\mathrm{ws},p}\rangle$
Rel	7.046	7.153	0.733	0.719	−66.376	−78.888	0.6321	0.6387
Non	7.096	7.239	0.630	0.632	−61.368	−72.759	0.7508	0.7207

relativistic ones, although their regions overlap. The solid lines express the mean values of the corresponding circles. It is seen that the value of the difference $\langle R_{\mathrm{ws},p}\rangle - \langle R_{\mathrm{ws},n}\rangle$ in the relativistic models is rather smaller than that in the non-relativistic models as in Table 5. Thus, the spread of the values of $R_{\mathrm{ws},\tau}$ in the non-relativistic models does not seem to cause the difference between δR in the two frameworks. The values of R_{coul} are indicated by the blue circles for reference.

Fig. 6 shows the values of $a_{\mathrm{ws},\tau}$. The straight lines stand for their average values. Those of the relativistic and non-relativistic models are distributed similarly over a wide region, but are small compared to $R_{\mathrm{ws},\tau}$, as $(a_{\mathrm{ws},\tau}/R_{\mathrm{ws},\tau})^2 \approx 0.01$. The difference between δR in the relativistic and non-relativistic models may not be due to these distributions of $a_{\mathrm{ws},\tau}$.

In Fig. 7 are shown the values of $m^*_{\mathrm{ws},\tau}$. The black circles represent those of the neutrons, the red circles the protons. The straight lines indicate their average values, which in the relativistic models are $\langle m^*_{\mathrm{ws},n}\rangle \approx 0.6321$ and $\langle m^*_{\mathrm{ws},p}\rangle \approx 0.6387$, and in the non-relativistic models $\langle m^*_{\mathrm{ws},n}\rangle \approx 0.7508$ and $\langle m^*_{\mathrm{ws},p}\rangle \approx 0.7207$. As seen in the figure, the circles of the relativistic models are almost at the same value and the ratio, $\langle m^*_{\mathrm{ws},p}\rangle/\langle m^*_{\mathrm{ws},n}\rangle$, is about 1.010, while those of the non-

Downloaded from https://academic.oup.com/ptep/article/2022/2/023D03/6507566 by Deutsches Elektronen Synchrotron DESY user on 23 March 2022

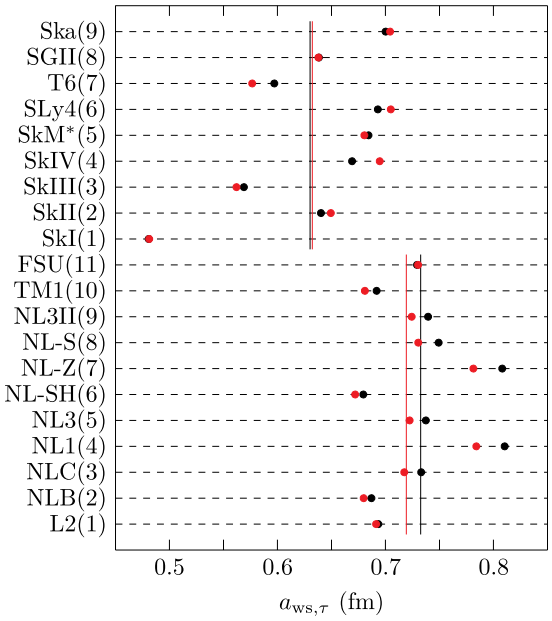

Fig. 6. The diffuseness parameters of the Woods–Saxon potentials for neutrons ($\tau = n$) and protons ($\tau = p$) in ^{208}Pb obtained from the relativistic and non-relativistic mean-field models. On the left-hand side, the relativistic and non-relativistic models used are indicated. The black circles represent the values of the diffuseness parameter $a_{\mathrm{ws},n}$, the red ones those of $a_{\mathrm{ws},p}$. The vertical lines indicate the average values of the corresponding circles in the relativistic and non-relativistic models, separately.

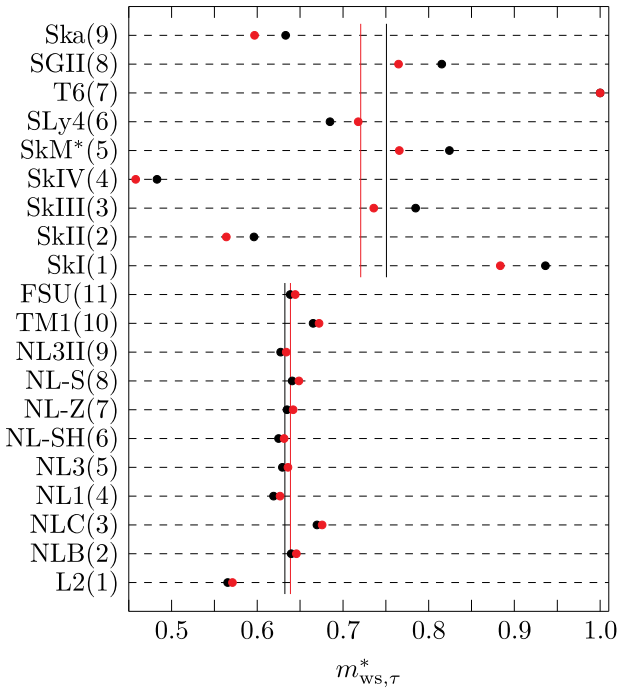

Fig. 7. The effective mass of neutrons ($\tau = n$) and protons ($\tau = p$) in ^{208}Pb obtained from the relativistic and non-relativistic mean-field models. On the left-hand side, the relativistic and non-relativistic models used are indicated. The black circles represent the values of the effective masses of neutrons, the red ones those of protons. In T6, the value for neutrons is the same as that for protons. The vertical lines indicate the average values of the corresponding circles in the relativistic and non-relativistic models, separately.

Downloaded from https://academic.oup.com/ptep/article/2022/2/023D03/6507566 by Deutsches Elektronen Synchrotron DESY user on 23 March 2022

Table 6. The mean values of the parameters for the Fermi-type neutron (n) and proton (p) distributions. They are obtained by approximating the densities in the relativistic and non-relativistic mean-field models for ^{208}Pb. The values of $\rho_{0,\tau}$ are given in units of fm^{-3} and those of $a_{\mathrm{den},\tau}$ and $R_{\mathrm{den},\tau}$ are in fm. For the definition of ϵ, see the text.

		$\rho_{0,\tau}$	$a_{\mathrm{den},\tau}$	$R_{\mathrm{den},\tau}$	ϵ
Rel	n	0.0860	0.553	6.903	0.1044
	p	0.0625	0.454	6.692	
Non	n	0.0911	0.554	6.766	0.0556
	p	0.0628	0.475	6.672	

Table 7. The mean values of the root msrs of the neutron (R_n) and proton (R_p) distributions and their difference ($\delta R = R_n - R_p$) obtained by the three approximations for ^{208}Pb. MF indicates the mean values in the relativistic and non-relativistic mean-field models, WS the ones obtained by approximating the mean-field potentials by Woods–Saxon potentials. Equation (57) stands for the equation number in the text used for the calculations of R_τ and δR given in that row. All the values are listed in units of fm. For details, see the text.

		R_n	R_p	δR
Rel	MF	5.749	5.466	0.283
	WS	5.740	5.457	0.283
	Eq. (57)	5.728	5.451	0.277
Non	MF	5.617	5.455	0.161
	WS	5.621	5.462	0.159
	Eq. (57)	5.629	5.460	0.169

relativistic models are spread out, as in nuclear matter, but the ratio in each model is almost the same and is on average $\langle m^*_{\mathrm{ws},p}\rangle/\langle m^*_{\mathrm{ws},n}\rangle \approx 0.9601$.

Table 5 lists the mean values of the WS parameters, the strengths of the one-body potentials, and the effective masses in the present simplified models for the relativistic and non-relativistic mean-field ones, respectively. It should be noticed that the values of $\langle m^*_{\mathrm{ws},\tau}\rangle$ and $\langle V_{\mathrm{ws},\tau}\rangle$ are almost the same as those of $\langle m^*_\tau\rangle$ and $\langle V_\tau\rangle$ in Table 2.

5.6 *The proton and neutron distributions*

It may be useful to see directly how the difference between δR is caused in terms of the neutron and proton densities. We approximate the neutron and proton distributions, $\rho_\tau(r)$, in the mean-field models by the Fermi-type function, which is widely employed [1,7]. The approximation is performed for

$$\rho_{\mathrm{ws},\tau}(r) \approx \rho_{0,\tau} f_\tau(r, R_{\mathrm{den},\tau}, a_{\mathrm{den},\tau}), \tag{56}$$

in the same minimization method as in Eq. (51). Since the obtained function satisfies the normalization $\int d^3r \rho_{\mathrm{ws},\tau}(r) = N_\tau$ with a small error of about 0.5%, we slightly correct $R_{\mathrm{den},\tau}$ to satisfy the normalization. We note that the correction by $\rho_{0,\tau}$ instead of $R_{\mathrm{den},\tau}$ yields almost the same values as those that will be seen in Tables 6 and 7. The minimization under the constraint on the nucleon number also yields similar results.

The msr, R^2_τ, by Eq. (56) is given as [1]

$$R^2_\tau \approx \frac{3}{5}\left(\frac{3N_\tau}{4\pi\rho_{0,\tau}}\right)^{2/3} + \pi^2 a^2_{\mathrm{den},\tau}, \tag{57}$$

Downloaded from https://academic.oup.com/ptep/article/2022/2/023D03/6507566 by Deutsches Elektronen Synchrotron DESY user on 23 March 2022

which provides the relationship between R_n^2 and R_p^2 as

$$R_n^2 = \frac{R_p^2 - \pi^2 a_{\mathrm{den},p}^2}{(1-\epsilon)^{2/3}} + \pi^2 a_{\mathrm{den},n}^2, \quad \epsilon = 1 - \frac{Z}{N}\frac{\rho_{0,n}}{\rho_{0,p}}. \tag{58}$$

When keeping order up to $O(\epsilon)$, the difference, $\delta R = R_n - R_p$, is written as

$$\delta R \approx \frac{\epsilon}{3} R_p + \frac{\pi^2}{2}\frac{a_{\mathrm{den},n}^2 - a_{\mathrm{den},p}^2}{R_p}. \tag{59}$$

Table 6 lists the average values of the parameters for the Fermi-type densities in Eq. (56) in the present relativistic and non-relativistic models. Table 7 shows the values of Eq. (57) using the results in Table 6. The average values of R_τ and δR in the mean-field models and their simplified versions are also listed in the rows called MF and WS, respectively. It is seen that the values in Eq. (57) and in WS almost reproduce the results of the mean-field models.

The values of the two terms on the right-hand side of Eq. (59) are given as

$$\delta R_{\mathrm{rel}} \approx 0.190 + 0.091 = 0.280\,\mathrm{fm}, \qquad \delta R_{\mathrm{non}} \approx 0.101 + 0.074 = 0.175\,\mathrm{fm}. \tag{60}$$

Thus the difference of about 0.1 fm between δR in the relativistic and non-relativistic models mainly comes from the first terms $\epsilon R_p/3$, and the diffuseness parameters yielding the second terms play a rather minor role. It should be noticed that the first term proportional to ϵ disappears when $\rho_{0,n} = (N/A)\rho$ and $\rho_{0,p} = (Z/A)\rho$.

Since the values of R_p and $\rho_{0,p}$ in the relativistic and non-relativistic models are almost the same, the difference between δR in Eq. (59) comes from $\rho_{0,n}$ in ϵ. Table 6 provides

$$\frac{(\rho_{0,n})_{\mathrm{rel}}}{(\rho_{0,n})_{\mathrm{non}}} = 0.944, \qquad \frac{(\rho_{0,p})_{\mathrm{rel}}}{(\rho_{0,p})_{\mathrm{non}}} = 0.995.$$

The 5.6% decrease of $(\rho_{0,n})_{\mathrm{rel}}$ provides the increase of $(R_n)_{\mathrm{rel}}$ by $0.944^{-1/3} = 1.019$, yielding the 0.1 fm difference that we are discussing. Fig. 2 shows qualitatively such a broadening of the neutron density in NL3, in comparison with that in Fig. 3.

In Table 2 are listed the mean values of the neutron and proton densities for the nuclear matter obtained by Eq. (37). Those values are almost the same as the corresponding ones in Table 6. They provide values of ϵ in Eq. (58) of 0.1138 and 0.0567 for the relativistic and non-relativistic models, respectively, which are comparable with the values for ^{208}Pb in Table 6. Thus, the various parameters including $\langle m_\tau^* \rangle$ and $\langle V_\tau \rangle$ at $r = 0$ for ^{208}Pb are similar to those for nuclear matter.

It may be noticed that the values listed in the MF rows in Table 7 are a little different from those of LSA in Table 4, since the former is the mean values of R_τ calculated by the models, while the latter has been obtained by a least-squares analysis of the calculated values compared with the experimental data [4].

6. The HVH lines in ^{208}Pb

In the previous section, we have shown that the mean values of $\langle m_\tau^* \rangle$, $\langle V_\tau \rangle$, and $\langle \rho_\tau \rangle$ in Table 2 for nuclear matter are almost the same as the corresponding ones in Tables 5 and 6 for ^{208}Pb. In order to explore the reason why δR in the relativistic and non-relativistic schemes are different from each other, the contributions from $R_{\mathrm{ws},\tau}$ and $a_{\mathrm{ws},\tau}$ in Figs. 5 and 6 to R_τ should also be examined, in addition to those from $V_{\mathrm{ws},\tau}$ and $m_{\mathrm{ws},\tau}^*$ in Figs. 4 and 7.

In the present section, first, it will be discussed that similar equations to Eqs. (9) and (10) hold for the dependence of R_τ on the WS parameters and $m_{\mathrm{ws},\tau}^*$ with the values in Figs. 4– 7. Second, the value of δR will be shown to be dominated by $m_{\mathrm{ws},\tau}^*$ and $V_{\mathrm{ws},\tau}$, rather than by $R_{\mathrm{ws},\tau}$

Downloaded from https://academic.oup.com/ptep/article/2022/2/023D03/6507566 by Deutsches Elektronen Synchrotron DESY user on 23 March 2022

Table 8. The mean values of the proportional constant B_τ between the root msr and the function of the Woods–Saxon parameters in Eq. (61). The standard deviation σ is given in parentheses. WS indicates the mean values using R_τ of the simplified models, while MF shows for reference those using R_τ of the full mean-field approximation. The numbers are written in units of $(\mathrm{fm}^2\mathrm{MeV})^{1/4}$. For details, see the text.

		$\langle B_\tau \rangle$ (σ)	
		WS	MF
Rel	n	5.295 (0.0063)	5.304 (0.0076)
	p	5.243 (0.0151)	5.253 (0.0151)
Non	n	5.288 (0.0217)	5.283 (0.0273)
	p	5.268 (0.0801)	5.261 (0.0685)

and $a_{\mathrm{ws},\tau}$. Third, it will be investigated whether or not the constraint on the values of $m^*_{\mathrm{ws},\tau}$ and $V_{\mathrm{ws},\tau}$ by the HVH theorem holds in the same way as in Fig. 1 for the nuclear matter. Finally, the difference between δR between the two schemes will be explained in terms of $m^*_{\mathrm{ws},\tau}$ and $V_{\mathrm{ws},\tau}$.

We discuss R_τ of the finite nucleus ^{208}Pb on the basis of Eqs. (9) and (10). For this purpose, first we examine if it is appropriate for Eqs. (9) and (10) to employ $m^*_{\mathrm{ws},\tau}$ and $V_{\mathrm{ws},\tau}$ defined in Eqs. (50) and (49). When R_τ calculated by the simplified models is expressed in terms of $m^*_{\mathrm{ws},\tau}$ and $V_{\mathrm{ws},\tau}$ as

$$R_\tau \approx B_\tau \left(-\frac{R^2_{\mathrm{ws},\tau}}{m^*_{\mathrm{ws},\tau} V_{\mathrm{ws},\tau}} \right)^{1/4} (1 + b_{\mathrm{ws},\tau})^{3/8}, \quad b_{\mathrm{ws},\tau} = \left(\frac{\pi a_{\mathrm{ws},\tau}}{R_{\mathrm{ws},\tau}} \right)^2, \tag{61}$$

then the value of the coefficient B_τ corresponding to B in Eq. (9) should be almost constant independently of the various interaction parameters of the mean-field models. In order to estimate the value of B_τ, both sides except for B_τ of the above equation are calculated for each model, according to Section 5. The results are listed on the left-hand side headed WS in Table 8, where the mean values of B_τ are shown as $\langle B_\tau \rangle$ in units of $(\mathrm{fm}^2\mathrm{MeV})^{1/4}$ in the relativistic and non-relativistic models, separately. The table shows that the values of the standard deviation (σ) are small enough for our purpose.

The meaning of B_τ may be qualitatively understood according to Ref. [1], where the values of C in Eq. (3) are estimated by summing a single particle radius over the occupied orbits in the HO potential. Their approximations yield values that are of the same order of magnitude as those of B_τ in Table 8, $B_n \approx 5.44$ for $N = 126$ and $B_p \approx 5.07$ for $Z = 82$ in units of $(\mathrm{fm}^2\mathrm{MeV})^{1/4}$.

We note that the values of σ for protons are larger than those for neutrons in both models. This fact may be due to the Coulomb potential, which is not explicitly taken into account on the right-hand side in Eq. (61). If $v_c = 22$ MeV is added to $V_{\mathrm{ws},p}$ by hand for reference, the values of σ for protons become comparable with those for neutrons: 0.0089 and 0.0217 in the relativistic and non-relativistic models, respectively. We expect, however, that these results do not change the following discussions on the difference between δR in the relativistic and non-relativistic models.

It should also be ensured that the 0.1 fm difference between δR is not due to the enhancement of $R_{n,\mathrm{rel}}$ by the factor $B_{n,\mathrm{rel}}$. The equation corresponding to Eq. (10) is described as

$$\frac{R_n}{R_p} = \frac{B_n}{B_p} \left(\frac{m^*_{\mathrm{ws},p} V_{\mathrm{ws},p}}{m^*_{\mathrm{ws},n} V_{\mathrm{ws},n}} \right)^{1/4} \left(\frac{R_{\mathrm{ws},n}}{R_{\mathrm{ws},p}} \right)^{1/2} \left(\frac{1 + b_{\mathrm{ws},n}}{1 + b_{\mathrm{ws},p}} \right)^{3/8}. \tag{62}$$

Since δR is written as $\delta R = R_p(R_n/R_p - 1)$ and the value of R_p is almost fixed due to the fitting in both relativistic and non-relativistic models, the difference between δR in the two frameworks

Downloaded from https://academic.oup.com/ptep/article/2022/2/023D03/6507566 by Deutsches Elektronen Synchrotron DESY user on 23 March 2022

stems from their values of R_n/R_p. Table 8 provides the ratio of $(\langle B_n\rangle/\langle B_p\rangle)_{\rm rel}/(\langle B_n\rangle/\langle B_p\rangle)_{\rm non} = 1.0061$. On the right-hand side of Table 8, the values of $\langle B_\tau\rangle$ in using R_τ from the mean-field calculations in Eq. (61) are listed. The table shows that the WS calculations yield almost the same results as those of the mean-field ones, $(\langle B_n\rangle/\langle B_p\rangle)_{\rm rel}/(\langle B_n\rangle/\langle B_p\rangle)_{\rm non} = 1.0055$. These values imply that the factor B_τ is not enough to explain the 0.1 fm difference. Thus, it is reasonable to use $V_{{\rm ws},\tau}$ and $m^*_{{\rm ws},\tau}$ defined in Eqs. (49) and (50) in the analysis of δR in ^{208}Pb.

Assuming that Eq. (62) holds for the mean values in Table 5, we have

$$R_n \approx \frac{B_n}{B_p}\left(\frac{\langle m^*_{{\rm ws},p}\rangle\langle V_{{\rm ws},p}\rangle}{\langle m^*_{{\rm ws},n}\rangle V_{{\rm ws},n}\rangle}\right)^{1/4}\left(\frac{\langle R_{{\rm ws},n}\rangle}{\langle R_{{\rm ws},p}\rangle}\right)^{1/2}\left(\frac{1+\langle b_{{\rm ws},n}\rangle}{1+\langle b_{{\rm ws},p}\rangle}\right)^{3/8} R_p \tag{63}$$

with $\langle b_{{\rm ws},\tau}\rangle = (\pi\langle a_{{\rm ws},\tau}\rangle/\langle R_{{\rm ws},\tau}\rangle)^2$. Using the values in Tables 5 and 8, the above equation provides for the relativistic and non-relativistic models, respectively, as

$$R_{n,{\rm rel}} \approx 1.0517\, R_{p,{\rm rel}}\,, \quad R_{n,{\rm non}} \approx 1.0274\, R_{p,{\rm non}}\,. \tag{64}$$

If we put the numbers of R_p obtained by the WS approximation in Table 7 into the right-hand sides of Eq. (64), then we have the values of $R_{n,{\rm rel}} \approx 5.739$ fm and $R_{n,{\rm non}} \approx 5.612$ fm. It is seen that they are almost the same values as those of the WS approximation in Table 7. Thus, Eq. (62) holds well also for the mean values in Tables 5 and 8.

Second, the value of δR will be shown to be dominated by $m^*_{{\rm ws},\tau}$ and $V_{{\rm ws},\tau}$, rather than by B_τ, $R_{{\rm ws},\tau}$, and $a_{{\rm ws},\tau}$, with the use of their mean values. One way to show this fact is by taking the numbers in Eq. (64) that imply that $R_{n,{\rm rel}} > R_{n,{\rm non}}$, when $R_{p,{\rm rel}} \approx R_{p,{\rm non}}$, indicating the 0.1 fm difference problem. Those numbers have been obtained by

$$1.0517 \approx 1.0468 \times 1.0047\,, \quad 1.0274 \approx 1.0329 \times 0.9947\,, \tag{65}$$

where the first numbers on the right-hand sides of the above equations come from the factor $(\langle m^*_{{\rm ws},p}\rangle\langle V_{{\rm ws},p}\rangle/\langle m^*_{{\rm ws},n}\rangle V_{{\rm ws},n}\rangle)^{1/4}$, the second numbers the rest of the factors in Eq. (63). Thus, the difference between R_n and R_p is mainly due to the first number coming from the values of $\langle m^*_{{\rm ws},\tau}\rangle$ and $\langle V_{{\rm ws},\tau}\rangle$ in both the relativistic and non-relativistic schemes. The second numbers from B_τ, $\langle R_{{\rm ws},\tau}\rangle$, and $\langle a_{{\rm ws},\tau}\rangle$ play a minor role in their differences. This fact also implies that the distribution of $R_{{\rm ws},\tau}$ and $a_{{\rm ws},\tau}$ over a wide region in Figs. 5 and 6 is not worrisome for the 0.1 fm problem. The minor role of $a_{{\rm ws},\tau}$ is consistent with the results of Eq. (60).

It may be seen in another way qualitatively that, compared to B_τ, $\langle R_{{\rm ws},\tau}\rangle$, and $\langle b_{{\rm ws},\tau}\rangle$, $\langle m^*_{{\rm ws},\tau}\rangle$ and $\langle V_{{\rm ws},\tau}\rangle$ play an important role in δR of the two frameworks. We write Eq. (61) in terms of the mean values,

$$R_{\tau,{\rm rel}} \approx B_{\tau,{\rm rel}}(-(\langle m^*_{{\rm ws},\tau}\rangle\langle V_{{\rm ws},\tau}\rangle)_{\rm rel})^{-1/4}(\langle R_{{\rm ws},\tau}\rangle_{\rm rel})^{1/2}(1+\langle b_{{\rm ws},\tau}\rangle_{\rm rel})^{3/8}, \tag{66}$$

for the relativistic scheme. In the above equation, keeping the values of $B_{\tau,{\rm rel}}$, $\langle R_{{\rm ws},\tau}\rangle_{\rm rel}$, and $\langle b_{{\rm ws},\tau}\rangle_{\rm rel}$, we replace $(\langle m^*_{{\rm ws},\tau}\rangle\langle V_{{\rm ws},\tau}\rangle)_{\rm rel}$ by that of the non-relativistic one, $(\langle m^*_{{\rm ws},\tau}\rangle\langle V_{{\rm ws},\tau}\rangle)_{\rm non}$. Then, the values of $R_{\tau,{\rm rel}}$ of the WS approximation in Table 7 and the mean values of Table 5 provide

$$R_{\tau,{\rm rel}}\left(\frac{\left(\langle m^*_{{\rm ws},\tau}\rangle\langle V_{{\rm ws},\tau}\rangle\right)_{\rm rel}}{\left(\langle m^*_{{\rm ws},\tau}\rangle\langle V_{{\rm ws},\tau}\rangle\right)_{\rm non}}\right)^{1/4} = \begin{cases} 5.607\,{\rm fm}, & \tau = n, \\ 5.403\,{\rm fm}, & \tau = p. \end{cases} \tag{67}$$

The above equation yields $\delta R = 5.607 - 5.403 = 0.204$ fm, which should be compared to $\delta R = 0.159$ fm in WS for the non-relativistic models in Table 7. The difference between δR in the two frameworks is reduced from $0.283 - 0.159 = 0.124$ fm to $0.204 - 0.159 = 0.045$ fm

Downloaded from https://academic.oup.com/ptep/article/2022/2/023D03/6507566 by Deutsches Elektronen Synchrotron DESY user on 23 March 2022

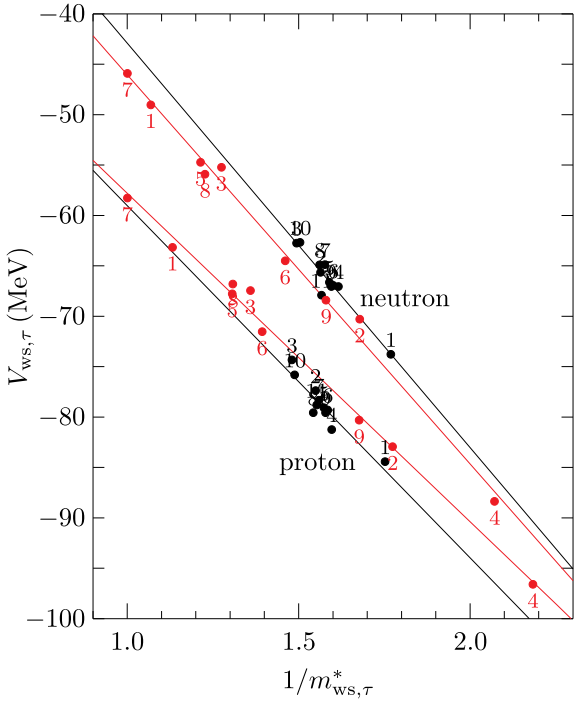

Fig. 8. The relationship between the effective mass and the one-body potential for neutrons ($\tau = n$) and protons ($\tau = p$) in the mean-field models for ^{208}Pb. The black circles show the values calculated by the 11 relativistic models, the red ones those by the 9 non-relativistic models. The least-square lines are shown for the four groups. The two black lines are obtained from the black circles for neutrons and protons, respectively, and the red lines from the red circles.

by 64%. Thus, it is seen that the 0.1 fm problem is closely related to the difference between $(\langle m^*_{\mathrm{ws},\tau}\rangle\langle V_{\mathrm{ws},\tau}\rangle)_{\mathrm{rel}}$ and $(\langle m^*_{\mathrm{ws},\tau}\rangle\langle V_{\mathrm{ws},\tau}\rangle)_{\mathrm{non}}$ in R_τ.

Third, let us investigate whether or not there is a constraint on $m^*_{\mathrm{ws},\tau}$ and $V_{\mathrm{ws},\tau}$ in ^{208}Pb, as in nuclear matter. In Fig. 8 are plotted the values of $V_{\mathrm{ws},\tau}$ in Fig. 4 and those of $m^*_{\mathrm{ws},\tau}$ in Fig. 7 in the $1/m^*_{\mathrm{ws},\tau}$–$V_{\mathrm{ws},\tau}$ plane. The black circles show the values for neutrons and protons in the relativistic models, the red circles those in the non-relativistic models. The numbers attached to each circle indicate the model used, according to the numbering mentioned in Section 4.2. A pair of the same number represents the values for neutrons and protons calculated by the same model.

The slanting lines are obtained by the least-squares method for the values of each group. The upper and lower black lines represent neutrons and protons in the relativistic models, respectively, the upper and lower red lines the non-relativistic models. It is remarkable that the values of each group follow the corresponding line well, and that the four lines are well separated from one another, as in Fig. 1 for nuclear matter. We notice that the only FSU(11) [16] among the relativistic models yields a point on the neutron line for the non-relativistic models. This may reflect the fact that FSU has added two additional parameters to the Lagrangian of, e.g., NL3(5) [22], so as to reduce the value of R_n. The values of the gradient ($a^{\mathrm{L}}_{\mathrm{ws},\tau}$) and the intercept ($b^{\mathrm{L}}_{\mathrm{ws},\tau}$) of the LSL,

$$V_{\mathrm{ws},\tau} = a^{\mathrm{L}}_{\mathrm{ws},\tau}/m^*_{\mathrm{ws},\tau} + b^{\mathrm{L}}_{\mathrm{ws},\tau}, \tag{68}$$

Downloaded from https://academic.oup.com/ptep/article/2022/2/023D03/6507566 by Deutsches Elektronen Synchrotron DESY user on 23 March 2022

Table 9. The values of the gradient ($a^{\rm L}_{{\rm ws},\tau}$) and the intercept ($b^{\rm L}_{{\rm ws},\tau}$) of the least-square line for the relationship between the depth of the one-body potential and the nucleon effective mass in Fig. 8. The numbers of $a^{\rm L}_{{\rm ws},\tau}$ and $b^{\rm L}_{{\rm ws},\tau}$ are given in units of MeV. The values of the correlation coefficient, r, are also listed. For details, see the text.

	Rel			Non		
	$a^{\rm L}_{{\rm ws},\tau}$	$b^{\rm L}_{{\rm ws},\tau}$	r	$a^{\rm L}_{{\rm ws},\tau}$	$b^{\rm L}_{{\rm ws},\tau}$	r
n	−40.120	−2.795	0.958	−38.609	− 7.438	0.997
p	−34.933	−24.098	0.937	−32.588	− 25.215	0.997

Table 10. The values for the combination composed of the effective mass and the coefficients of the least-square line for asymmetric nuclear matter (the first column) and for ^{208}Pb (the third column) in the relativistic and non-relativistic models. The values of the product of the effective mass and the strength of the one-body potential are also listed in the second column for ^{208}Pb. All the numbers are given in units of MeV. For details, see the text.

		$\langle a_\tau\rangle + \langle b_\tau\rangle\langle m^*_\tau\rangle$	$\langle m^*_{{\rm ws},\tau}\rangle\langle V_{{\rm ws},\tau}\rangle$	$a^{\rm L}_{{\rm ws},\tau} + b^{\rm L}_{{\rm ws},\tau}\langle m^*_{{\rm ws},\tau}\rangle$
Rel	n	−41.814	−41.956	−41.887
	p	−49.737	−50.386	−50.324
Non	n	−44.321	−46.075	−44.193
	p	−51.364	−52.437	−50.760

are listed in Table 9 for relativistic (Rel) and non-relativistic (Non) models. The values of the correlation coefficient, r, are also shown, which are nearly equal to 1.

In Fig. 8, it is seen that the variation of the effective mass and the strength of the one-body potential in finite nuclei is also constrained in a similar way to that in Fig. 1 for nuclear matter. Equation (68) has the same form as Eq. (44) from the HVH theorem. Thus, the HVH theorem seems to be inherent in the mean-field approximation for finite nuclei too. From now on, we will refer to the LSL of ^{208} Pb as the HVH line.

We compare the coefficients of the HVH line for ^{208}Pb in Table 9 to those of Eq. (44) for nuclear matter listed in Table 2. The coefficients of Eq. (44) are shown to be constrained by the HVH theorem through Eq. (47). It is seen in Tables 2 and 9 that the values of the corresponding coefficients are not the same as each other, but the magnitude relations of the corresponding two values are almost the same as those of the other pair. More important values for the present discussion are those in Eq. (47). In the first column in Table 10 is listed one of the values in Eq. (47), $\langle a_\tau\rangle + \langle b_\tau\rangle\langle m^*_\tau\rangle$, and the corresponding values obtained from Tables 5 and 9 are given in the second and the last columns. It is seen that the values for nuclear matter in the first column are almost the same as those for ^{208}Pb in the other columns. Since the values in the first column are nothing but the results due to the HVH theorem, it is confirmed that those in the second and third columns also reflect the constraint by the theorem.

We note that the values of the first column have been obtained by introducing a model with v_c in Eq. (38). This is done so as to provide neutrons and protons with the same average binding energies by Eq. (37), as in stable nuclei. The value of v_c is employed that approximately corresponds to the energy of the Coulomb potential for ^{208}Pb in Eq. (42). Although the model has been used as a guide for discussions of the finite nucleus, Table 10 shows conversely that

Downloaded from https://academic.oup.com/ptep/article/2022/2/023D03/6507566 by Deutsches Elektronen Synchrotron DESY user on 23 March 2022

Table 11. The neutron (n) and proton (p) potentials at the mean value of the effective mass. The numbers are given in units of MeV. For details, see the text.

	$V^{\rm rel}_{{\rm ws},\tau}(\langle m^*_\tau\rangle_{\rm rel})$	$V^{\rm non}_{{\rm ws},\tau}(\langle m^*_\tau\rangle_{\rm rel})$	$V^{\rm non}_{{\rm ws},\tau}(\langle m^*_\tau\rangle_{\rm non})$
n	−66.264	−68.517	−58.865
p	−78.792	−76.238	−70.434
$V_n - V_p$	12.528	7.721	11.569

such a simple model almost reproduces the results for finite nuclei and is useful for describing asymmetric nuclear matter.

In Fig. 8, it should be noticed that, on the one hand, the distance between the two black lines for the relativistic models is about 12.5 MeV at a fixed value of $1/m^*_{{\rm ws},\tau}$, as listed in Table 11. This is almost the same as the mean value of $V_3 = V_{{\rm ws},n} - V_{{\rm ws},p}$ in Fig. 4. This is because of $m^*_{{\rm ws},n} \approx m^*_{{\rm ws},p}$ in the relativistic models. On the other hand, in the non-relativistic models, the distance between the two red lines for the same value of $1/m^*_{{\rm ws},\tau}$ is about 7.7 MeV, in spite of the fact that $V_3 \approx 11.6$ MeV as in Table 11. This is because, in the non-relativistic models, the value of the neutron effective mass is larger than that of the proton one, except for SLy4(6) [24], as in Fig. 7. The value of $V_3 \approx 11.6$ MeV is approximately kept by providing neutrons and protons with different effective masses. As seen below, it is essential for understanding the 0.1 fm difference that the values of the effective mass for neutrons are different from the ones for protons in the non-relativistic models, while those in the relativistic models are almost the same.

So far, understanding the dependence of R_τ on $m^*_{{\rm ws},\tau}$ and $V_{{\rm ws},\tau}$ is simply based on their mean values as in Eqs. (65) and (67), aiming to emphasize their roles in the 0.1 fm problem. Finally, we investigate the roles of of $m^*_{{\rm ws},\tau}$ and $V_{{\rm ws},\tau}$ in R_τ by using their values themselves, together with the HVH line in Fig. 8.

Equation (67) has been obtained by replacing the mean values $(\langle m^*_{{\rm ws},\tau}\rangle\langle V_{{\rm ws},\tau}\rangle)_{\rm rel}$ by $(\langle m^*_{{\rm ws},\tau}\rangle\langle V_{{\rm ws},\tau}\rangle)_{\rm non}$. In order to explore in more detail how the value of R_τ in the relativistic scheme approaches that in the non-relativistic one by changing $m^*_{{\rm ws},\tau}$ and $V_{{\rm ws},\tau}$, we replace the values of $m^*_{{\rm ws},\tau}$ and $V_{{\rm ws},\tau}$ in R_τ in each relativistic model by $\langle m^*_{{\rm ws},\tau}\rangle_{\rm non}$ and $\langle V_{{\rm ws},\tau}\rangle_{\rm non}$. The replacement will be made keeping the values of $R_{{\rm ws},\tau}$ and $b_{{\rm ws},\tau}$ in each model, and using the HVH line in Fig. 8. By this procedure, we will see the roles of $m^*_{{\rm ws},\tau}$ and $V_{{\rm ws},\tau}$ in R_τ separately, as follows.

In Fig. 9 is shown R_τ as a function of $m^*_{{\rm ws},\tau}$ in the case of NL3(5) as an example. The closed and open circles indicate the values of R_τ in the full mean-field calculation and in the simplified one in Section 5, respectively, at the value of $m^*_{{\rm ws},\tau}$ for NL3. The solid curves are calculated by keeping the values of $R_{{\rm ws},\tau}$ and $a_{{\rm ws},\tau}$ of NL3 and using $V_{{\rm ws},\tau}$ given by the HVH line for the relativistic models in Fig. 8. The closed and open circles are seen to be almost on the curves. The dashed curves also show R_τ, but using $V_{{\rm ws},\tau}$ given by the HVH line for the non-relativistic models in Fig. 8.

In Fig. 9, we have specified six points on the curves, where X_n, Y_n, and Z_n are for the neutrons, and others for the protons. The points X_τ indicate the positions of the open circles. The points Y_τ and Z_τ are on the dashed curves. The former indicates the place where NL3 provides $m^*_{{\rm ws},\tau}$, and the latter the place of $m^*_{{\rm ws},\tau} = \langle m^*_{{\rm ws},\tau}\rangle_{\rm non}$ as shown by the vertical lines. The replacement of $m^*_{{\rm ws},\tau}$ and $V_{{\rm ws},\tau}$ in NL3 by $\langle m^*_{{\rm ws},\tau}\rangle_{\rm non}$ and $\langle V_{{\rm ws},\tau}\rangle_{\rm non}$ is made by using the values at point Z_τ. We made, however, the replacement in two steps according to the curves in Fig. 9. In the first

Downloaded from https://academic.oup.com/ptep/article/2022/2/023D03/6507566 by Deutsches Elektronen Synchrotron DESY user on 23 March 2022

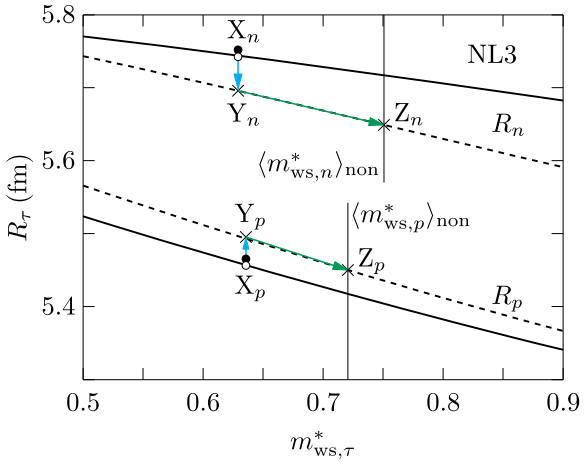

Fig. 9. The root msr as a function of the effective mass for $\tau = n$ and $\tau = p$ in NL3. The closed circles are obtained by the full mean-field approach, and the open ones by the simplified Hamiltonian of NL3. The solid curves are calculated by using the least-square lines for the relationship between $m^*_{\mathrm{ws},\tau}$ and $V_{\mathrm{ws},\tau}$ in the relativistic models in Fig. 8, the dashed ones by using those in the non-relativistic models. The top two lines are for neutrons, and the bottom two ones for the protons. In these curves, the values of the Woods–Saxon parameters, $R_{\mathrm{ws},\tau}$ and $a_{\mathrm{ws},\tau}$, are taken from those determined by NL3. The vertical lines indicate the average values of the effective masses for neutrons ($\langle m^*_{\mathrm{ws},n}\rangle_{\mathrm{non}}$) and protons ($\langle m^*_{\mathrm{ws},p}\rangle_{\mathrm{non}}$) in the non-relativistic models. The point X_n indicates the place of the open circle for the neutrons, Y_n the point on the dashed curve at the same value of $m^*_{\mathrm{ws},n}$ as that for X_n. The point Z_n shows the intersection point between the dashed curve and the vertical line for $\langle m^*_{\mathrm{ws},n}\rangle_{\mathrm{non}}$. The points X_p, Y_p, and Z_p are given in a similar way. The blue and green arrows are used for discussions in the text.

step, the values at X_τ are replaced by those at Y_τ, and in the second step the values at Y_τ are replaced by those at Z_τ. This process is shown in Fig. 9 by the arrows. The blue arrow indicates the first step, the green one the second step. In this way, we may see how R_τ in NL3 varies by $m^*_{\mathrm{ws},\tau}$ and $V_{\mathrm{ws},\tau}$ separately and approaches R_τ in the non-relativistic scheme.

Fig. 9 shows that the value of R_n is decreased in the first step, because $V_{\mathrm{ws},n}$ becomes deeper as seen in Fig. 8. From Y_n to Z_n, the potential becomes shallower, but the value of the effective mass is increased and the role of the kinetic part as a repulsive potential declines. As a result, the value of R_n further shrinks, as in Fig. 9. The decrease of R_τ from Y_τ to Z_τ with increasing $m^*_{\mathrm{ws},\tau}$ is understood qualitatively by Eqs. (61) and (68), which yield

$$m^*_{\mathrm{ws},\tau} = -\frac{1}{b^{\mathrm{L}}_{\mathrm{ws},\tau}}\left(a^{\mathrm{L}}_{\mathrm{ws},\tau} + \frac{B^4_\tau}{R^4_\tau}R^2_{\mathrm{ws},\tau}(1+b_{\mathrm{ws},\tau})^{3/2}\right). \tag{69}$$

Thus, the value of R_n in the relativistic models approaches that in the non-relativistic models, following the path under the constraint of the HVH theorem on $V_{\mathrm{ws},\tau}$ and $m^*_{\mathrm{ws},\tau}$.

With respect to R_p, Fig. 9 shows its increase from X_p to Y_p, because of the decreasing strength of $|V_{\mathrm{ws},p}|$. From Y_p to Z_p, the value of R_p decreases in the same way as that of R_n from Y_n to Z_n, according to Eq. (69). The final value of R_p at the point Z_p almost returns to its original value at X_p, since the value of R_p at X_p for the relativistic model is fixed by the experimental value of R_c as an input, while the value at Z_p is almost equal to the values of R_p for the non-relativistic models that are fixed in the same way.

In the above analysis, it should be noticed that the value of $\langle m^*_{\mathrm{ws},n}\rangle_{\mathrm{non}}$ is larger than that of $\langle m^*_{\mathrm{ws},p}\rangle_{\mathrm{non}}$ in Table 5. Owing to this fact, the path from Y_n to Z_n is longer than that from Y_p to Z_p as seen in Fig. 9. This difference also works to make R_n smaller in the path from Y_n to Z_n.

Downloaded from https://academic.oup.com/ptep/article/2022/2/023D03/6507566 by Deutsches Elektronen Synchrotron DESY user on 23 March 2022

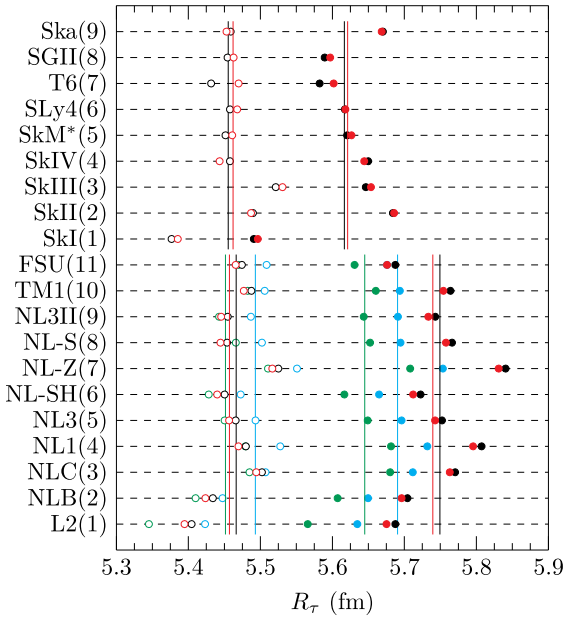

Fig. 10. The root msr R_τ of ^{208}Pb calculated in the relativistic and non-relativistic models. On the left-hand side, the models used are indicated. The black closed and open circles are obtained by the full mean-field approximations for the neutrons ($\tau = n$) and protons ($\tau = p$), respectively. The red ones are obtained by the simplified Hamiltonian for each model. The blue ones are obtained through the first step discussed in the text, the green ones by the second step. The vertical lines show the average values of the same color circles, respectively. For details, see the text.

Fig. 10 shows the values of R_τ that are obtained by the same procedure as in Fig. 9 for all the relativistic mean-field models taken in the present paper. The black and red circles show the results of the full mean-field calculations and the simplified ones in Section 5, respectively, where the closed circles are for neutrons and the open circles for protons. The vertical lines indicate their mean values. It is seen that the simplified calculations reproduce well the values of R_τ by the full calculations. Those for the non-relativistic models are also shown in the same way.

The blue circles are obtained by the first step from X_τ to Y_τ mentioned in Fig. 9, the green ones by the second step. All the models show a similar change of R_τ to that in Fig. 9 such that the values of R_n decrease by two steps, while those of R_p come back to almost the same values by the second step from Y_τ to Z_τ.

Fig. 11 shows the values of δR, using the same designating symbols as in Fig. 10. The values from the two steps shown by the green circles are almost the same as the blue ones obtained by the first step, since the values of R_p return to the original ones by the second step.

The results of R_τ and δR in Figs. 10 and 11 are summarized in Table 12 in units of fm. The mean values of R_τ in the relativistic models are listed in the columns headed Red, Blue, and Green according to the colors of those figures. From Red to Green, the value of R_n decreases, while that of R_p increases from Red to Blue and decreases from Blue to Green, up to almost the Red one, as shown in the figures. In changing the values V_τ and m^*_τ in the relativistic models following the HVH lines, the value of δR shrinks from 0.283 fm to 0.193 fm, which should be compared to 0.159 fm for the non-relativistic models. The difference between δR in the relativistic and non-relativistic models becomes smaller by 73%, changing its value from 0.124 fm to 0.034 fm.

Downloaded from https://academic.oup.com/ptep/article/2022/2/023D03/6507566 by Deutsches Elektronen Synchrotron DESY user on 23 March 2022

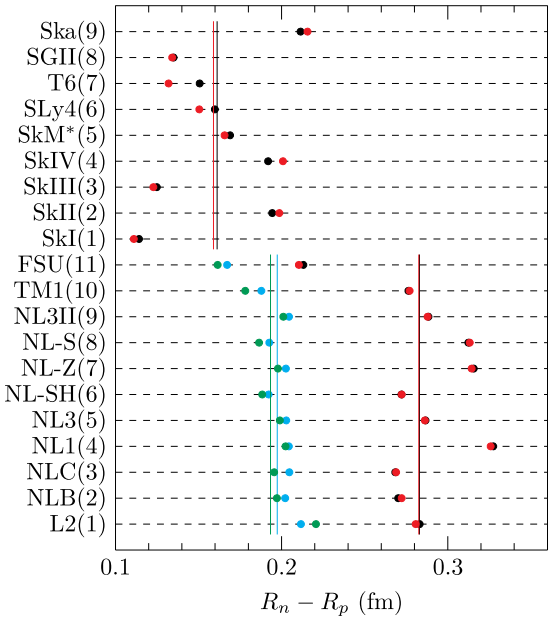

Fig. 11. The difference between the root msrs of the neutron and proton distributions in ^{208}Pb calculated in the relativistic and non-relativistic models. On the left-hand side, the models used are indicated. The black closed circles are obtained by the full mean-field approximations, and the red ones by the simplified Hamiltonian for each model. The blue ones are obtained through the first step, the green ones through the second step discussed in the text. The vertical lines show the average values of the same color circles, respectively. For details, see the text.

Table 12. The average values of the root msr of the proton and neutron distributions in the relativistic (Rel) and non-relativistic (Non) models in various approximations. Red, Green, and Blue indicate the average values corresponding to those in Figs. 10 and 11, respectively. All the numbers are given in units of fm. For details, see the text.

	Rel			Non
	Red	Blue	Green	Red
R_n	5.740	5.691	5.645	5.621
R_p	5.457	5.493	5.452	5.462
δR	0.283	0.197	0.193	0.159

It is concluded that most of the 0.1 fm difference between δR in the relativistic and non-relativistic models is attributed to the difference between the values of their V_τ and m^*_τ, which are constrained by $\rho_{0,\tau}$ through the HVH theorem. The remaining difference may be caused by the sum of many small contributions, in addition to those from $R_{\mathrm{ws},\tau}$, $a_{\mathrm{ws},\tau}$, and B_τ, from the approximations used. The exchange term of the Coulomb force, the center of mass correction, the small component of the wave functions, etc., are also managed differently in the two frameworks. Discussions of these effects, however, are beyond the present purpose.

7. Summary

Reference [4] has pointed out that the neutron skin thickness defined by $\delta R = R_n - R_p$ in ^{208}Pb is larger by about 0.1 fm in the relativistic mean-field models than in the non-relativistic ones. Here, R_n and R_p represent the root msr (mean-square-radius) of the point neutron and

Downloaded from https://academic.oup.com/ptep/article/2022/2/023D03/6507566 by Deutsches Elektronen Synchrotron DESY user on 23 March 2022

proton distributions in the nucleus, respectively. The value of the charge radius R_c of ^{208}Pb is about 5.503 fm. The 0.1 fm difference is small for neither nuclear physics [1,10,17,18], nor astrophysics [3,5,18]. In this paper, we have investigated why the difference is avoidable in the present mean-field models, even though both relativistic and non-relativistic models are constructed phenomenologically with free parameters to be fixed by experimental values.

The value of R_p is one of the most important inputs, together with the binding energy per nucleon and the Fermi momentum in nuclear matter in all of the phenomenological models [14,24]. The relationship between R_p and R_c is unambiguously defined theoretically [8], and the latter is observed experimentally through electromagnetic probes, whose reaction mechanisms are well understood [6,7,9]. Hence, the 0.1 fm problem is due to the difference between the values of R_n in the two frameworks.

It is shown that the values of R_τ are dominated by those of $(-m^*_\tau V_\tau)^{-1/4}$, as in Eq. (61), where m^*_τ and V_τ represent the effective mass in units of M and the strength of the one-body potential near the center of the nucleus ($r \approx 0$), respectively, and the subscript indicates $\tau = p$ for protons and $\tau = n$ for neutrons. Although m^*_τ and V_τ are complicated functions of the interaction parameters in the phenomenological models, they are not independent of each other. Their variations are constrained together with the nucleon density ρ_τ at $r \approx 0$ by the Hugenholtz–Van Hove (HVH) theorem [19–21].

In writing the average values of m^*_τ and V_τ in each framework as $\langle m^*_\tau \rangle$ and $\langle V_\tau \rangle$, respectively, their product is approximately expressed by the HVH equation as $\langle m^*_\tau \rangle \langle V_\tau \rangle \approx a_\tau + b_\tau \langle m^*_\tau \rangle$, where a_τ and b_τ are constants. The values of a_τ and b_τ depend on the average values of $\rho_\tau(\langle \rho_\tau \rangle)$, the binding energy per nucleon $E_{\rm B}$, and Coulomb energy v_c of the corresponding asymmetric nuclear matter with N and Z. Since the values of $E_{\rm B}$ and v_c are almost the same in the relativistic and non-relativistic models, the difference between the two frameworks on the right-hand side of the HVH equation is attributed to the difference between the values of $\langle \rho_\tau \rangle$ and $\langle m^*_\tau \rangle$. Indeed, the values of $\langle \rho_\tau \rangle$ and $\langle m^*_\tau \rangle$ in the nuclear matter in Table 2 are almost the same as those for ^{208}Pb in Tables 5 and 6. The difference on the right-hand side of the HVH equation for the two frameworks is expressed by $\langle m^*_\tau \rangle \langle V_\tau \rangle$ on the left-hand side, which induces the difference of R_n between the relativistic and non-relativistic models, according to Eq. (61).

Table 10 provides their average values as $(\langle m^*_n \rangle \langle V_n \rangle)_{\rm non} = -46.075\,{\rm MeV}$ for the non-relativistic models against $(\langle m^*_n \rangle \langle V_n \rangle)_{\rm rel} = -41.956\,{\rm MeV}$ for the relativistic models. The ratio of these values yields

$$(46.075/41.956)^{1/4} = 1.0237,$$

which is comparable to the value showing the 0.1 fm difference of R_n as

$$R_{n,{\rm rel}}/R_{n,{\rm non}} = 5.740/5.621 = 1.0212$$

in Table 7. This comparison assumes the same relationship between the average values of R_n and $(-m^*_n V_n)^{-1/4}$ as in Eq. (61). The results of the more detailed analysis without using the average values are summarized in Table 12, which shows that about 70% of the 0.1 fm difference is explained according to the HVH theorem.

We note that the 0.1 fm problem is observed using the limited number of Skyrme-type interactions and relativistic mean-field models in Ref. [4], so the problem has been investigated with the same models in the present paper. It may be interesting to explore other phenomenological models [2] to identify whether or not there is a similar difference problem and the HVH theorem is useful for understanding the difference.

Downloaded from https://academic.oup.com/ptep/article/2022/2/023D03/6507566 by Deutsches Elektronen Synchrotron DESY user on 23 March 2022

The 0.1 fm difference has also been observed in ^{48}Ca in Ref. [4]. It could be discussed in a similar way to ^{208}Pb in the present paper, but a new method must be devised for comparing the results for ^{48}Ca with those for nuclear matter in the mean-field models.

Acknowledgments

The authors would like to thank Professor T. Suda for useful discussions.

References

[1] A. Bohr and B. R. Mottelson, Nuclear Structure (World Scientific, Singapore, 1998), Vol. **1**.
[2] X. Roca-Maza, M. Centelles, X. Viñas, and M. Warda, Phys. Rev. Lett. **106**, 252501 (2011).
[3] M. Thiel et al., J. Phys. G: Nucl. Part. Phys. **46**, 093003 (2019).
[4] H. Kurasawa, T. Suda, and T. Suzuki, Prog. Theor. Exp. Phys. 2021, 013D02(2021).
[5] D. Adhikari et al., Phys. Rev. Lett. **126**, 172502 (2021).
[6] T. deForest and J. D. Walecka, Adv. Phys. **15**, 1 (1966).
[7] H. De Vries, C. W. De Jager, and C. De Vries, At. Data Nucl. Data Tables **36**, 495 (1987).
[8] H. Kurasawa and T. Suzuki, Prog. Theor. Exp. Phys. **2019**, 113D01 (2019).
[9] J. D. Bjorken and S. D. Drell, Relativistic Quantum Mechanics (McGraw-Hill, New York, 1964).
[10] T. Suda and H. Simon, Prog. Part. Nucl. Phys. **96, 1** (2017).
[11] H. J. Emrich, Ph.D. Thesis, Johannes-Gutenberg-Universität, Mainz (1983).
[12] S. Abrahamyan et al., Phys. Rev. Lett. **108**, 112502 (2012).
[13] J. R. Stone et al., Phys. Rev. C **68**, 034324 (2003).
[14] B. D. Serot and J. D. Walecka, Advances in Nuclear Physics, eds. E. Vogt Vogt and J. Negle Negle (Plenum, New York, 1986), Vol. **16**.
[15] B. D. Serot and J. D. Walecka, Int. J. Mod. Phys. E **6**, 515 (1997).
[16] B. G. Todd-Rutel and J. Piekarewicz, Phys. Rev. Lett. **95**, 122501 (2005).
[17] E. Chabanat et al., Nucl. Phys. A **627**, 710 (1997).
[18] G. Hargen et al., Nat. Phys. **12**, 186 (2016).
[19] H. A. Bethe, Phys. Rev. **103**, 1353 (1956).
[20] V. F. Weisskopf, Nucl. Phys. **3**, 423 (1957).
[21] N. M. Hugenholtz and L. Van Hove, Physica **24**, 363 (1958).
[22] G. A. Lalazissis, J. Köning, and P. Ring, Phys. Rev. C **55**, 540 (1997).
[23] M. J. Giannoni and P. Quentin, Phys. Rev. C **21**, 2076 (1980).
[24] E. Chabanat et al., Nucl. Phys. A **635**, 231 (1998); **643**, 441(E) (1998) [erratum].
[25] D. Vautherin and D. M. Brink, Phys. Rev. C **5**, 626 (1972).
[26] D. Vretenar et al., Phys. Rev. C **68**, 024310 (2003).
[27] M. Brack, C. Get, and H.-B Hakansson, Phys. Rep. **123**, 275 (1985).
[28] P. G. Reinhard et al., Z. Phys. A **323**, 13 (1986).
[29] M. M. Shama, M. A. Nagarajan, and P. Ring, Phys. Lett. B **312**, 377 (1993).
[30] M. Rufa et al., Phys. Rev. C **38**, 390 (1988).
[31] P. G. Reinhard, Z. Phys. A **329**, 257 (1988).
[32] Y. Sugahara and H. Toki, Nucl. Phys. A **579**, 557 (1994).
[33] M. Beiner et al., Nucl. Phys. A **238**, 29 (1975).
[34] J. Bartel et al., Nucl. Phys. A **386**, 79 (1982).
[35] E. Chabanat et al., Nucl. Phys. A **627**, 710 (1997)
[36] N. V. Giai and H. Sagawa, Phys. Lett. B **106**, 379 (1981).
[37] H. S. Köhler, Nucl. Phys. A **258**, 301 (1976).
[38] P.-G. Reinhard, X. Roca-Maza, and W. Nazarewicz, Phys. Rev. Lett. **127**, 232501 (2021).

Downloaded from https://academic.oup.com/ptep/article/2022/2/023D03/6507566 by Deutsches Elektronen Synchrotron DESY user on 23 March 2022